Minireview: Biophysical Mechanisms of Cell Membrane Sonopermeabilization. Knowns and Unknowns

Jean-Michel Escoffre, Ayache Bouakaz

Mini-review - Biophysical mechanisms of cell membrane sonopermeabilization: Knowns and unknowns.

Jean-Michel Escoffre and Ayache Bouakaz

UMR 1253, iBrain, Université de Tours, Inserm, Tours, France.

KEYWORDS

Ultrasound – microbubbles – sonoporation – sonopermeabilization – bioeffects - biophysical stimuli.

ABSTRACT (200 Words)

Microbubble-assisted ultrasound has emerged as a promising method for the delivery of low molecular weight chemotherapeutic molecules, nucleic acids, therapeutic peptides and antibodies *in-vitro* and *in-vivo.* Its clinical applications are under investigations for local delivery drug in oncology and neurology. However, the biophysical mechanisms supporting the acoustically-mediated membrane permeabilization are not fully established. This review describes the present state of the investigations concerning the acoustically-mediated stimuli (*i.e.,* mechanical, chemical and thermal stimuli) as well as the molecular and cellular actors (*i.e.,* membrane pores, endocytosis) involved in the reversible membrane permeabilization process. The different

hypotheses, which were proposed to give a biophysical description of the membrane permeabilization, are critically discussed.

1. INTRODUCTION

In modern pharmacology, the main research goal is to design drug delivery methods to efficiently increase drug extravasation without harming healthy cells and tissues[1]. The general aim of such systems is based on the reversible disruption of biological barriers such as blood vessel walls (*i.e.*, drug extravasation) and cell membranes (*i.e.*, intracellular uptake of drugs), thus enhancing the local delivery of therapeutic molecules across these barriers and improving their therapeutic efficacy at the desired site while minimizing side effects to healthy tissues[2]. The therapeutic efficacy of delivered drug is dependent on the quantity of affected cells and on the intracellular concentration of drugs while *in-vivo*, it is conditional on the treated tissue volume and on the intratissue bioavailability (*i.e.*, concentration and biodistribution) of drugs[1, 2].

The combination of high frequency ultrasound (0.5 – 10 MHz) and contrast agents (*i.e.*, consisting of gas microbubbles) was introduced as a promising method for drug delivery[3]. In the literature, this combination was referred to as *microbubble-assisted ultrasound*, *sonoporation* or *sonopermeabilization*[4, 5]. Since the mid 90's, the feasibility and great potential of this modality has been reported in an increasing number of publications on *in-vitro* and *in-vivo* delivery of a wide range of therapeutic molecules, including low molecular weight chemotherapeutic drugs (*i.e.*, < 4 kDa)[6-8], nucleic acids (*i.e.*, plasmid DNA, siRNA, mRNA)[9-11], therapeutic proteins[12, 13], antibodies[14, 15] and cells[16, 17]. Under the guidance of various imaging modalities (*e.g.*, ultrasound or magnetic resonance imaging)[18-21], the acoustic effects may be spatially and temporally controlled, leading thus to a non-invasive targeting a tissue volume of superficial tissues (*e.g.*, skin)[22] and deeply embedded organs (*e.g.*, liver, pancreas, brain)[6, 7]. Microbubble-assisted

ultrasound is currently attracting great biomedical interest for the treatment of a wide range of diseases including cancers[6, 23, 24], neurological disorders[13, 25, 26], cardiovascular diseases[27] and hind-limb ischemia[28].

The overall delivery efficacy of therapeutic molecules is strongly dependent on the interaction between ultrasound waves, microbubbles and cells[29]. The microbubbles, which are formulated as biocompatible shelled micrometer sized gas bodies in aqueous suspension, are commonly mixed with cells for *in-vitro* studies or administered by intravascular/intratissue injection for *in-vivo* evaluations[30]. The microbubble response to ultrasound waves stimulation depends on many factors including ultrasound (*e.g.*, frequency, acoustic pressures, pulse duration) and microbubble (*e.g.*, size, physical properties of the core and shell) properties[29]. *In-vivo*, environmental conditions such as hydrostatic pressure and dissolved gas saturation are also among the influencing factors[31]. The gas core of a microbubble has a compressibility that is several orders of magnitude greater than an equivalent volume of blood. The association of this high compressibility with the low density of the core provides a substantial impedance mismatch between the microbubbles and the surrounding medium, and makes microbubbles responsive to ultrasound[32]. At low acoustic amplitudes, the microbubbles oscillate (*i.e.*, expansion and contraction) in a symmetrical and linear way, in response to the alternating of the compression and rarefaction phases of ultrasound wave[29, 32]. At higher acoustic pressures, the microbubbles adopt a non linear acoustic behavior, reflected in a lengthening of a larger expansion amplitude of the microbubbles in comparison to their compression[32]. This acoustic phenomenon is termed *stable* or *non inertial cavitation*. At much higher acoustic pressures, microbubbles oscillate more vigorously, resulting in their violent collapse and destruction[29, 32]. This acoustic process is designated as the *inertial cavitation*. Both acoustic cavitations lead to biophysical effects such as mechanical, chemical and thermal stimuli,

which transiently increase the permeability of biological barriers (*i.e.*, endothelial barriers, cell plasma membranes), thus enhancing the extravasation and the intracellular uptake of drugs[4, 5, 33].

In this review, we give an overview of the state-of-the-art knowledge on acoustically-mediated biophysical stimuli (*i.e.*, mechanical, chemical and thermal stimuli) and subsequently on molecular and cellular structures responsible for the membrane permeabilization. The limitations and future developments of microbubble-assisted ultrasound will be further discussed.

2. BIOPHYSICAL PROCESSES

2.1. MECHANICAL STIMULI

2.1.1. Pulling/pushing process

Under stable cavitation, the microbubble oscillations are at the origins of two mechanical stimuli: (i) *pulling/pushing process* (also familiarly termed *cell massage*) and (ii) *microstreaming*. Van Wamel *et al.*, investigated the interaction between oscillating microbubbles and cell plasma membrane using ultrafast, real-time optical microscopy[34]. They reported that stably oscillating microbubbles (1 MHz, PNP 0.4 MPa), closely located to the plasma membrane of cells, were able to gently push and pull the plasma membrane, generating a critical transmembrane shear force (**Figure 1**). This mechanical stress led to a rapid membrane deformation and the formation of pores once the membrane breakdown threshold is exceeded. Every cell deformed by stably oscillating microbubbles showed an intracellular uptake of propidium iodide (*i.e.*, non-permeant and fluorescent dye used for the assessment of membrane permeabilization), suggesting that only deformed cell displayed an induced membrane permeability. However, no correlation between the amount of dye uptake and the magnitude of the microbubble oscillation was observed. Kooiman *et al.*, demonstrated that the use of targeted microbubbles required much lower acoustic pressures (1 MHz, PNP 80-200 kPa) for the permeabilization of the plasma membrane, in comparison with

bare microbubbles[35, 36]. These results can be explained by the close bond of targeted microbubbles with plasma membrane. The authors reported a positive correlation between the efficacy of membrane permeabilization and the oscillation amplitudes of the targeted microbubbles[35].

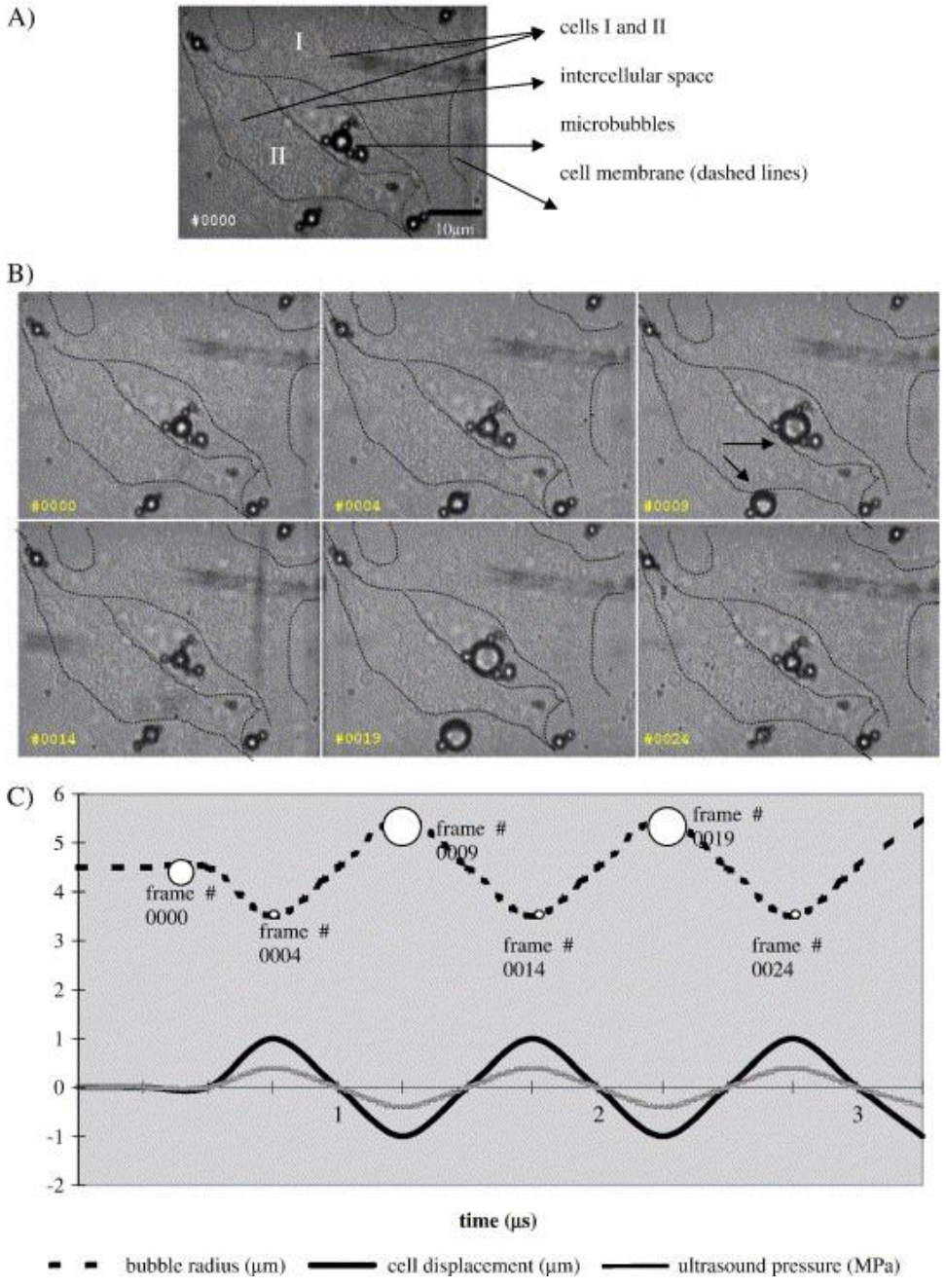

Figure 1. Pulling/pushing process. A. First frame of a Brandaris recording in which contours (membranes) of the cells are drawn (dashed lines). Two cells can be distinguished as well as the intercellular space and the microbubbles. B. Brandaris recording: 6 selected frames out of a total of 128 frames. The pushing and pulling behavior of the vibrating microbubbles nearby the cells is shown (1 MHz, 50 Hz PRF, 10 cycles, 0.4 MPa PNP, 5s). Cell I was not

deformed, cell II was deformed (arrows in frame 0009). C. Plotted are the relations between the ultrasound pressure wave, microbubble radius (expansion/compression), and cell II displacement. Frame numbers correspond to the frame numbers in B. (Adapted with permission from Van Wamel *et al.*,[34] - Copyright © 2006 Elsevier B.V.)

2.1.2. Microstreaming

At higher acoustic pressures, the microbubbles adopt a nonlinear acoustic behavior of microbubbles, expressed by a large expansion phase of the microbubbles[32]. Such microbubble behavior gives rise to non linear components at multiples of the transmitted frequency, the so-called harmonic components. This acoustic regime is the basis of modern ultrasound contrast imaging methods[33]. These stable oscillations lead to local steady fluid flow surrounding the microbubble, a process named *microstreaming*[37, 38]. When the oscillating microbubbles are in close vicinity of biological barriers, such microstreaming results in shear stresses on these membranes. Collis *et al.,* investigated the microstreaming patterns generated around a microbubble using microscopic particle-image velocimetry, albeit microbubbles are larger than contrast agent microbubbles (**Figure 2**) [39]. They demonstrated that each microstreaming pattern was related to a specific oscillation mode of the microbubble, and change in microstreaming patterns was achieved by modifying the ultrasound frequency. Each microstreaming pattern also resulted in different shear stress and stretch/compression distributions surrounding the microbubble. Microstreaming patterns displayed significant changes around the microbubble, indicating acoustically-mediated membrane permeabilization may be either enhanced or inhibited in different areas across the plasma membrane. The level of shear stress clearly depends on a large set of ultrasound and microbubble parameters[37, 39]. The shear stress related to microstreaming is relatively high (*i.e.,* 100 to 1000 Pa) compared to the shear stress associated with blood flow (*i.e.*, 0.1 to 4 Pa)[37].

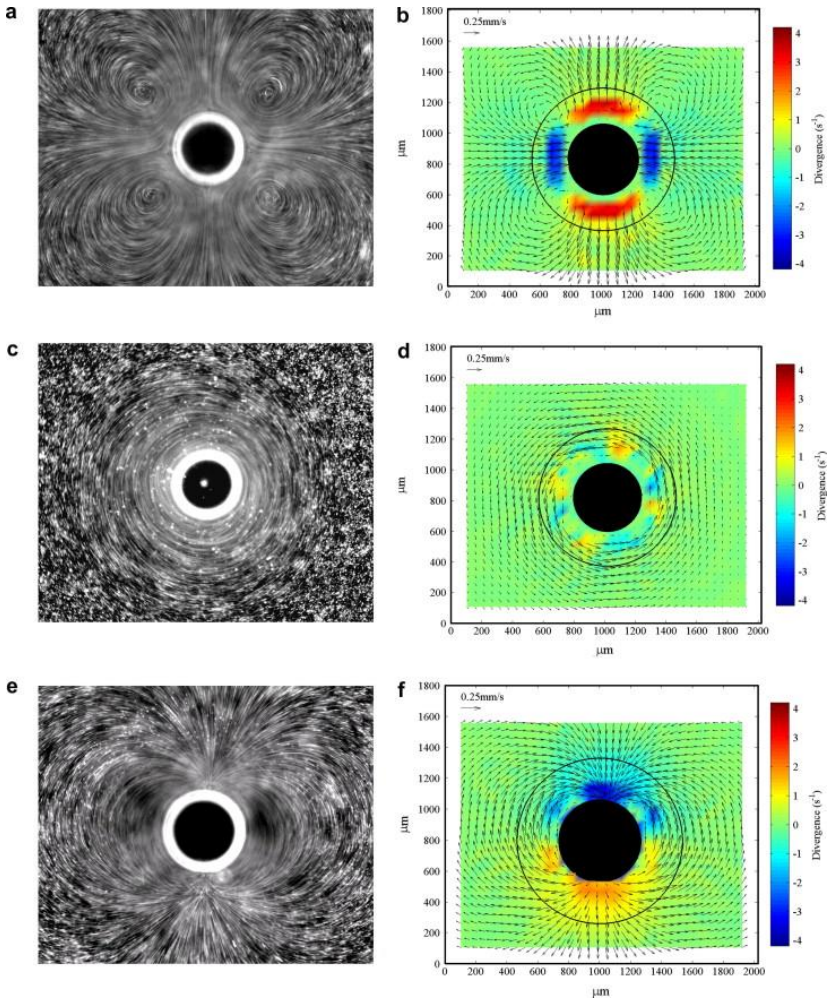

Figure 2. Microstreaming. Quadrupole microstreaming pattern created by linear translation of a 232 µm radius bubble attached to a horizontal surface and forced at 2.422 kHz at 30 V p-p; (a). streak image, (b). PIV velocity vector field and divergence (positive divergence zones at top and bottom of black circle representing bubble, negative zones at left and right). Circular vortex microstreaming pattern created by circular translation of a 224 µm radius bubble on surface forced at 1.188 kHz at 30 V p-p, (c). streak image, (d). PIV velocity vector field and divergence (color version online; weak positive and negative divergence alternate around bubble circumference). Dipole microstreaming pattern created by radial oscillation of a 267 µm radius bubble on surface forced at 8.658 kHz at 30 V p-p, (e). streak image, (f). PIV velocity vector field and divergence (negative divergence zone at top, positive below). (Adapted with permission from Collis *et al.*[39] – Crown Copyright © 2009 Published by Elsevier B.V.).

Similar figures have been reported theoretically by Wu *et al.*, showing that the exposure of free microbubbles to low acoustic pressures (2 MHz, 0.1 MPa PNP) resulted in shear stress of 92 Pa while at high acoustic pressures (2 MHz, 0.4 MPa PNP), the shear stress increased strongly to 1100 Pa[40]. Doinikov and Bouakaz described the shear stress distribution created on the cell plasma membrane by adjacent oscillating contrast microbubbles[41]. The shear stress was negligible at the

point, which was the projection of the microbubble center on the cell plasma membrane, then it increased, being directed away from the microbubble, reached a maximum, decreased down to zero and changed sign and getting directed to the microbubble afterwards. As a result, the maximum of the shear stress on the cell plasma membrane occurred along a circle whose radius is about 0.287*d*, where *d* is the distance between the microbubble and the cell. This maximum value is likely to determine the threshold value of shear stress which leads to the onset of membrane permeabilization. Recently, Chen *et al.*, reported that a microbubble activated at low acoustic pressure (1 MHz, 0.2 MPa PNP) in a microvessel could generate a shear stress of up to 26.95 kPa on the vessel wall, which should be high enough to damage the vascular endothelial cells[42].

The microstreaming-mediated shear stress could lead to membrane deformation and/or membrane disruption by tearing the cell plasma membrane open[37, 38, 43]. Such changes in the structure of the cell plasma membrane have been mainly reported on lipid vesicles[44] and cells[45, 46]. Indeed, Moosavi Nejad *et al.*, investigated the dynamics of lymphoma cell and microbubble interaction using high-speed real-time imaging and theoretical analyses[46]. They described that stably oscillating microbubbles (0.834 MHz, 0.12 MPa) induced microstreaming and imposed 35.3 Pa shear stress on the cell plasma membrane. This stress caused a reversible plasma membrane permeabilization, subsequently leading to the intracellular delivery of plasmid DNA. In addition, microstreaming locally pulled the cell plasma membrane, resulting in transient local membrane microprotrusion[46]. Other experimental investigations[47, 48] and numerical simulations[49, 50] of such microstreaming effects are available for *in-vitro* scenarios, however, there is still a lack of experimental assessments of microstreaming generated *in-vivo*, and clearly investigations need to be carried out.

2.1.3 Shock waves

At much higher acoustic pressures, microbubbles grow quickly during the rarefaction phase, and then undergo a violent collapse during the compression phase leading to their fragmentation (*i.e.,* inertial cavitation) (**Figure 3**)[51].

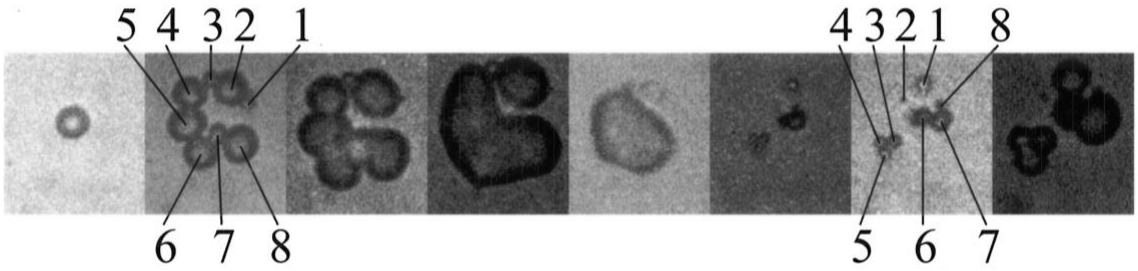

Figure 3. Ultrasound-induced microbubble fragmentation. Ultrasound parameters: 0.5 MHz, 10 cycles, 0.67 MPa PNP. Interframe times for frames: 0.33 μs. Each image frame corresponds to a 23 × 23 μm^2 area. (Adapted with permission from Postema *et al.*[51] – Copyright © 2004 World Federation for Ultrasound in Medicine and Biology. Published by Elsevier Inc.).

This acoustic process can release highly concentrated energy, also known as *shock waves*, where the associated local high acoustic pressure and shear stress may impact the permeabilization of plasma membrane[52]. Kodama *et al.,* reported that cell plasma membrane was permeabilized following the interaction with the shock wave when cells were located at more than 5 μm away from the center of microbubble[53]. The pressure of the shock wave inversely decreased with increasing propagation distance (*i.e.,* distance between microbubble and cell). Steinbach *et al.,* demonstrated that the cell plasma membrane was most sensitive to the characteristics of shock waves propagating through the membrane and intracellular components[54]. Because each cell type may show differences in membrane composition (*i.e.,* lipid, protein and carbohydrates) and in intracellular densities that could influence the membrane fluidity[55], the magnitude of the shock wave-induced surface velocity may be different for each cell type, resulting in different membrane permeabilization efficacy. Koshiyama *et al.,* performed molecular dynamics simulations of the interaction of shock waves with lipid bilayers[56]. They reported that shock waves decreased the

thickness of bilayer and increased the lateral fluidity of lipids[56]. The most important structural changes in the lipid bilayers were the lateral displacement of lipid headgroups and tilts of lipid molecules, which were observed only in the external monolayer of the lipid bilayer directly exposed to shock waves[57]. These changes in physicochemical properties of the cell plasma membrane increased thus the penetration of water molecules into the hydrophobic region of the lipid bilayers[56-58]. When the initial number of water molecules in the hydrophobic region exceeded a critical value, the bilayer-water system spontaneously developed into a water-filled pore structure, also named hydrophilic pore[58]. The increase in the initial number of water molecules enhanced the probability of pore formation into the lipid bilayer.

Most experimental investigations reported that the exposure of cells to higher acoustic pressures led to microbubble collapsing and subsequently to membrane permeabilization to exogenous molecules through the formation of membrane pores[52, 59-61]. Qiu *et al.,* reported that collapsing microbubbles (1 MHz, PNP 2.2 MPa) caused a transient permeabilization of cell plasma membrane, subsequently the intracellular delivery of PEI:pDNA complexes across membrane pores[52]. In addition to pore formation, a smoother and flatter cell surface[62] as well as a decrease in cell size[59] were observed using SEM. Although most of *in-vitro* studies reported SEM and AFM data to prove the formation of membrane pores, it cannot be ruled out that membrane invaginations which are actually endocytic vesicles, are formed in response to microbubble-mediated ultrasound. Using SEM and TEM, Zeghimi *et al.,* reported that the exposure of cells to collapsing microbubbles increased the membrane permeability to exogenous compounds through the stimulation of caveolae-dependent endocytosis for two thirds of the recorded event, with the remaining one third related to caveola-independent endocytosis (*i.e.,* clathrin-dependent

endocytosis, micropinocytosis, macropinocytosis) or to non-specific pathways such as membrane pores[63].

2.1.4. Microjetting

The asymmetrical collapse of the microbubble occurs at higher acoustic pressures and might be responsible for the generation of acoustic jets. The microbubble collapse occurs nearby a physical barrier such as a cell plasma membrane. This collapse propels the fluid in which the microbubble is immersed through the microbubble wall and in this case, the velocity of the upper microbubble wall exceeds the velocity of the lower microbubble wall[64, 65]. Subsequently, the fluid volume above the microbubble is accelerated and focused during the asymmetrical collapse, resulting in the formation of a high-speed liquid microjet that projects toward the barrier[51]. This microjet hits the lower microbubble wall, leading to a funnel-shaped protrusion that finally impacts the barrier. This acoustic phenomenon is called *microjetting*[64, 65]. The impact of a microjet on a cell plasma membrane causes a high-pressure area. Cook *et al.,* termed this pressure as the water-hammer pressure[66]. The microjet-induced damage can be estimated by comparing the water-hammer pressure with the maximum stress ($\tau_{max} << 200\ kPa$) that the impact area can withstand before rupture[51]. If the water-hammer pressure of a microjet exceeds this stress, the microjet will be able to permeabilize or perforate plasma membrane[64]. Using high-speed real-time imaging, Postema *et al.*, reported that the exposure of an encapsulated microbubble (R = 8.43 μm) to high acoustic pressure (0.5 MHz, 0.85 MPa) induced the formation of an acoustic microjet (**Figure 4**)[51], which had traveled over a length of 26.2 μm in 0.33 μs, providing an average microjet velocity of 79.4 $m.s^{-1}$. The microjet volume is approximately of 60 femtoliters. In these experimental conditions, such a jet may penetrate cell plasma membrane because the water-hammer pressure is around 60 MPa and therefore higher than $\tau_{max} << 200$ kPa[51].

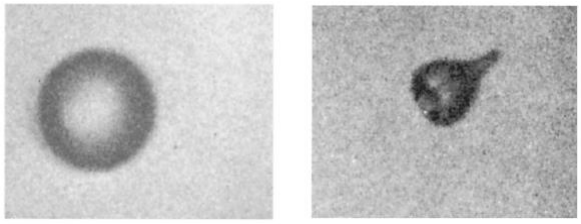

Figure 4. Ultrasound-induced microjet development. The ultrasound parameters: 0.5 MHz, 10 cycles, MI 1.2, exposure time of 10 ns. (Adapted with permission from Postema *et al.*[51] – Copyright © 2004 World Federation for Ultrasound in Medicine and Biology. Published by Elsevier Inc.).

Previous experimental studies described that the exposure of cells to higher acoustic pressures in presence of microbubbles resulted in the microbubble collapse and subsequently to the formation of high speed microjet, which permeabilized cell plasma membrane to fluorescent dyes and drugs through the formation of membrane pores[67, 68]. Such changes in the permeability of cell plasma membrane have been mainly reported on adherent cells[65, 67, 68]. Prentice *et al.*, reported that under high acoustic pressures (1 MHz, 0.5 MPa PNP), microbubbles underwent inertial cavitation and collapse with the outermost microbubble hemisphere generating a microjet directed at the cell monolayer[67]. The authors investigated the post-insonation membrane consequences of microjets using AFM. Microjetting events induced the formation of single deep micro-sized pits at the plasma membrane level[67]. While no evidence of intracellular uptake of dye and cell viability have been reported, the formation of microjet-induced pits was compatible with a water-hammer pressure (4 MPa) which exceeded τ_{max} (3 kPa)[67]. In agreement with previous studies[51, 64, 65, 67], Kudo *et al.*, reported that the exposure of microbubbles to high acoustic pressures (1 MHz, 1.1 MPa PNP) resulted in high-speed liquid microjets during the nonlinear contraction of microbubbles using high-speed camera[68]. Real-time optical observations and successive SEM observation revealed that such microjets transiently increased the membrane permeability of endothelial cells to propidium iodide through the formation of micron-sized membrane perforations at the microbubble location[68].

2.2. CHEMICAL STIMULI

Reactive oxygen species (ROS) play major a role in the normal physiological functions. However, the dysregulation of the homeostasis of ROS, especially excessive production of ROS, are associated with the pathophysiology of several diseases[69, 70]. The formation of ROS could play also a key role in the acoustically-mediated permeabilization of biological barriers through the oxidation of phospholipids and lipoproteins[71, 72]. <Juffermans *et al.*, investigated whether H_2O_2 is involved in the reversible permeabilization of rat cardiomyoblasts after ultrasound exposure at low acoustic MI (1.8 MHz, MI 0.1 or 0.5, during 10 s), in the presence of stable oscillating microbubbles, by measuring the production of H_2O_2 and intracellular calcium influx (*i.e.*, monitoring of membrane permeabilization)[73]. They reported that the shear stress from acoustically-mediated microbubble oscillations led to a significant increase in intracellular H_2O_2 level about 1 hour after exposure to ultrasound at both MIs 0.1 and 0.5. Furthermore, they reported concomitant increase in intracellular calcium levels at both MIs in the presence of microbubbles, which was not detected in the absence of extracellular calcium. Moreover, this calcium influx was fully inhibited at MI 0.1 and partially reduced at MI 0.5 in the presence of catalase (*i.e.*, H_2O_2 scavenger), suggesting a close relationship between membrane permeabilization (*i.e.*, calcium influx) and H_2O_2 formation. Recently, new investigations confirmed the positive correlation between the production of ROS and the enhanced permeabilization of plasma membrane[5, 74]. Phospholipids, main membrane components, are very susceptible to the attack by acoustically-generated ROS[75]. The presence of oxidized phospholipids is able to change membrane properties, especially with regards to membrane permeability. The oxidation of phospholipids leads to an important conformation change in the phospholipids[76]. This conformational change results in an increase in the average area per lipid and a decrease of the bilayer thickness, especially evident at

high concentrations of oxidized phospholipids. Water defects are then created in the membrane, thus increasing its permeability to small molecules including water and ions[76]. This permeability increases with the concentration of oxidized phospholipids. Moreover, Lionetti *et al.*, reported that the exposure of endothelial cells to ultrasound at high mechanical index (1.6 MHz, MI 1.2) without microbubbles led to a selective enhancement of caveolar-dependent endocytosis, partially mediated by ROS generation[77]. However, it cannot be excluded that the presence of microbubbles can increase the production of ROS and by that enhances the caveolar-dependent endocytosis. Using molecular dynamics simulations, Escoffre *et al.*, reported that ROS can form inside the microbubbles after exposure to ultrasound[78]. These radicals could easily then diffuse through the microbubble shell toward the surrounding aqueous phase and participate to the peroxidation and permeabilization of nearby plasma membrane. The same study confirmed experimentally that the exposure of microbubbles to ultrasound (1 MHz, 400 kPa PNP) induced the production of ROS, which can be inhibited by the presence of ROS scavengers/inhibitors in the surrounding medium. Using flow cytometry, they demonstrated that the presence of ROS scavengers/inhibitors, during the sonoporation, significantly decreased the transfection level without loss of cell viability. All together, these results suggest that the exposure of microbubbles to ultrasound might be the origin of chemical effects, which play a role in the *in-vitro* permeabilization of cell membrane when generated in its proximity.

2.3. THERMAL STIMULI

Even if the role of the thermal stimulus in the sonopermeabilization of biological barriers is still subject to debate, it cannot be ruled out that such stimulus is a contributing factor[4]. Indeed, Wu *et al.*, reported that the exposure of microbubbles to ultrasound (2 MHz, 0.4 W/cm^2) induced a local rise in temperature of about 2°C in 10 seconds[79]. In this regard, it is important to mention that any

acoustically-mediated temperature increase could change the physicochemical properties of the cell plasma membrane and could render them more sensitive to membrane deformation and/or the membrane breakdown. Indeed, phospholipid membranes were observed to be leaky to polar molecules due to mismatches between liquid crystal and solid-state domains at the thermal phase transition[80, 81]. Conductance fluctuations were reported and were indicative of pathways for ionic species[82, 83]. The fluctuating properties of these currents were indicative of the lack of regular ionic channels but much more of membrane defects in the phospholipid membranes. This is very similar to what was described in the electrophysiological experiments. Further experimental investigations as well as molecular dynamic simulations should be considered in order to clearly establish the role of the thermal stimulus in the membrane permeabilization.

3. TRANSMEMBRANE PATHWAYS FOLLOWING SONOPERMEABILIZATION

3.1. MEMBRANE PORES

3.1.1. Formation of membrane pores

All experimental data indicated that sonopermeabilization induced the formation of plasma membrane pores and this process took place within several tens of microseconds, almost synchronously with stable or inertial cavitation[34, 68, 84-86]. Stably cavitating microbubbles in the direct contact or in the close vicinity of cell plasma membrane induces the formation of membrane hydrophilic pores as a result of both mechanical and chemical stimuli[34, 40, 87]. Nevertheless, the non-specific membrane pores generated by mechanical stimuli induce a calcium influx which cannot be prevented by free radical scavengers (*e.g.,* catalase)[73, 74, 88] or ion channel blockers (*e.g.,* iberiotoxin, verapamil)[88]. Based on the intracellular uptake of non-permeant fluorescent molecules[35, 74, 89] and by assessing changes in membrane electrophysiology[88, 90], previous investigations indicated that the intracellular delivery of exogenous compounds through membrane

pores is likely governed by passive diffusion or by ultrasound-mediated propulsion (*i.e.*, microstreaming, acoustic radiation force). Indeed, Fan *et al.*, reported that only cells adjacent to stably oscillating microbubbles (1 MHz, 0.27 MPa PNP) exhibited an enhanced intracellular uptake of propidium iodide[91]. Since the cell plasma membrane with hydrophilic pores act as molecular sieve for the intracellular uptake of exogenous molecules, the size of these pores has been estimated by delivering fluorescently-labeled markers (*e.g.*, dextran, beads) of different sizes into the cells and by assessing their incorporation using fluorescence imaging[89, 92, 93]. Current investigations reported that the size of membrane pores ranges from several tens of nanometers to a few hundreds of nanometer[45, 59, 94]. Such pores were generated at low acoustic pressures (1 MHz, 0.1-0.5 MPa PNP) and their size and/or their number increased with increasing acoustic pressure and exposure time[45, 95, 96]. However, Karshafian *et al.*, showed that pore size as large as 56 nm (which correspond to 2 MDa fluorescently-labelled dextran) were created independently of the acoustic pressure (0.5 MHz, 125-570 kPa PNP)[93]. In contrast, Meijering *et al.*, described that macromolecules with a size above 155 kDa did not freely diffuse through membrane pores at low acoustic pressure (1 MHz, 0.22 MPa PNP) but were mainly endocytosed[89]. The lifetime of the membrane pores is in the order of milliseconds to few seconds, immediately after switching off the ultrasound emitter[59, 90, 94]. Van Wamel *et al.*, described that the rapid decay in the permeabilization of cell plasma membrane indicated that membrane pores exists as long as the oscillating microbubbles were present[34].

Based on optical techniques (SEM, AFM, flow cytometry)[5, 52] and electrophysiological assessments[90, 97-99] of cell plasma membrane, previous investigations reported that collapsing microbubbles led also to membrane pores at higher acoustic pressures (0.5-2 MHz, >0.5 MPa PNP). Few studies demonstrated that the efficiency of acoustically-mediated membrane

permeabilization and the cell viability were positively correlated with the inertial cavitation dose, ICD (*i.e.*, corresponding to the spectral broadband signal enhancement during microbubble destruction)[52, 100]. Qiu *et al.*, reported that the ICD generated during microbubbles exposure is affected by ultrasound parameters including PNP, PRF and insonation time[52]. They showed that the efficacy of *in-vitro* PEI:pDNA delivery was linearly enhanced with the increasing ICD through the formation of membrane pores. However, this process was observed only when an ICD threshold was overcome. Then, the pDNA transfection efficacy reached a plateau while the ICD kept increasing[52]. The cell viability significantly declined when the IC activity was further increased, thus preventing the pDNA expression. The assessment of ICD should predict the efficacy and the reversibility of acoustically-mediated membrane permeabilization[52, 100]. Based on optical imaging (fluorescence microscopy, SEM and AFM), current studies showed that inertial cavitation-induced membrane pores were larger then pores reported during stable cavitation[61, 67], with pore sizes in the few hundreds of nanometer to few micrometer range (**Figure 5**)[52, 61, 67].

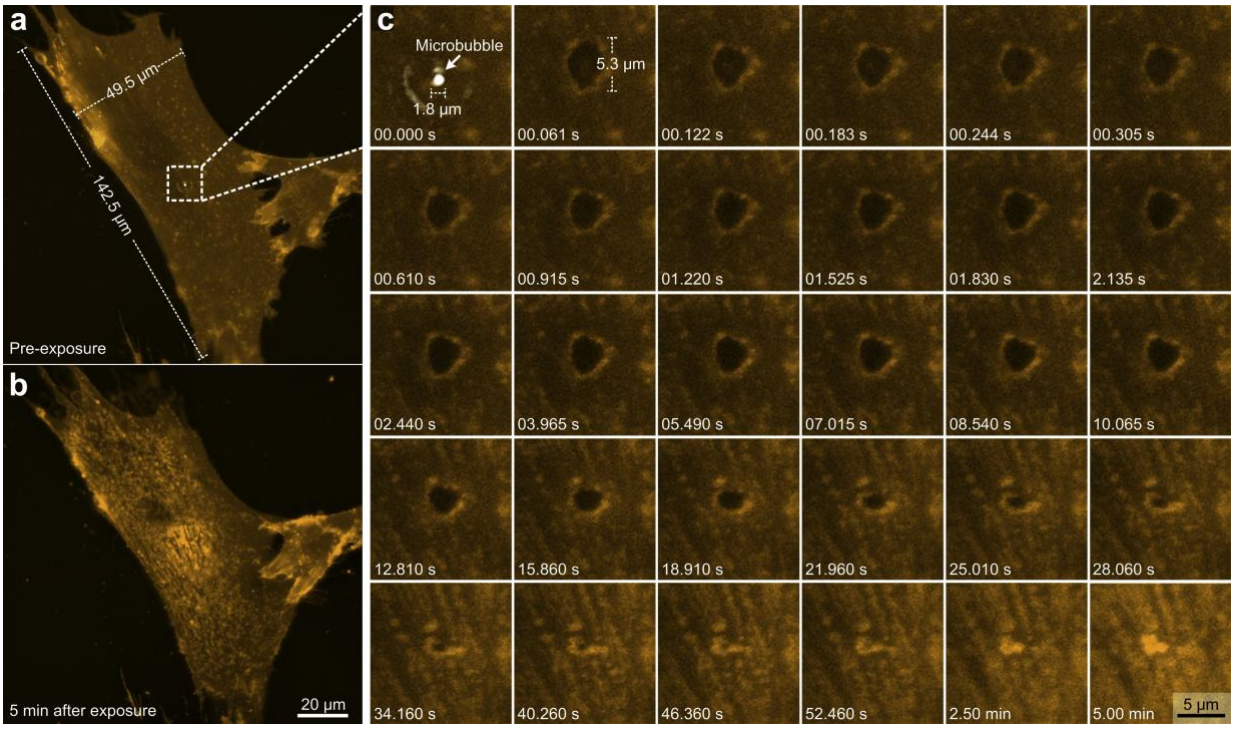

Figure 5. Time-series confocal fluorescence images revealing localized membrane perforation and recovery induced by ultrasound-triggered collapse of a single microbubble. (a, b) Whole-cell images of a fibroblast (a) before exposure and (b) 5 min after exposure (1 MHz, 10 cycles, 0.85 MPa PNP, exposure time of 10 μs). The scan plane was centered at the apical surface of the cell. The membrane is indicated by orange fluorescence; the microbubble is depicted by the overlaid gray-scale contrast. (c) Series of membrane fluorescence images centered about the microbubble adhered to the cellular membrane (Adapted with permission from Hu *et al.*[85] – Copyright © 2013 World Federation for Ultrasound in Medicine and Biology. Published by Elsevier Inc.).

In addition, the pore size was positively correlated with acoustic parameters, specifically the acoustic pressure[52, 60, 84]. This correlation confirmed other investigations which reported an increase in intracellular uptake of exogenous molecules with increasing acoustic pressure[92, 93]. Although SEM and AFM images depicted larger membrane pores on post-insonation cell samples, it cannot be ruled out that small membrane pores were formed. Indeed, such pores might have quickly resealed during the period required for the preparation of cell samples. Similarly to the pore size, the lifetime of membrane pores which have been described as a result of inertial cavitation was longer than for pores reported for stable cavitation. Actually, the lifetime of large membrane pores is in the range of seconds to few minutes, immediately after ultrasound is turned off[84, 95].

In conclusion, all investigations described that the formation of membrane pores can be temporally and spatially well controlled by adjusting the acoustic parameters (*i.e.*, PNP, PRF, insonation time)[52, 68, 84, 89, 98] and microbubble related parameters (*i.e.*, doses, types, microbubble/cell distance)[98, 101] in order to increase the delivery of exogenous molecules while minimizing irreversible cell damages[52, 100].

3.1.2. Resealing of membrane pores

Upon exposure to microbubble-assisted ultrasound, the cells progressively recover their initial physiological state. This biological process consists of two sequential steps: the resealing of membrane pores and the cell recovery[5]. The resealing of membrane pores is a rapid and short-term

process (*i.e.*, several minutes) whereas the cell recovery is a long-term step (*i.e.*, several hours). The different kinetics of the pore resealing depends on the ultrasound conditions (*i.e.*, ultrasound parameters, microbubble dose, *etc.*), the cell physiology (*i.e.*, adherent cells, cell suspension) and the sensitivity of assay used to assess the pore resealing (*e.g.*, patch-clamp techniques, intracellular uptake of fluorescent dyes)[73, 90, 98, 102].

The membrane resealing of small pores (tens of nanometers) relies on a passive process, automatically mediated by the spontaneous reorganization of phospholipids into their thermodynamically most stable state[103, 104]. This biophysical process should be facilitated by the acoustically-induced disassembly of actin cytoskeleton[105, 106]. Indeed, the presence and the contraction of the subcortical actin cytoskeleton is known to prevent the spontaneous membrane resealing because both processes exert forces in opposite directions[103].

Mammalian cells can also sense and interpret such acoustically-mediated calcium influx as an immediate danger signal[103]. These cells then activate other calcium-dependent mechanisms to reseal the small and large membrane pores. Thus, an ATP- and calcium-dependent process, termed as *exocytosis,* has been described for the membrane resealing of large pores (from few hundreds of nanometers to few micrometers) [60, 97]. The current knowledge of this process in the post-sonoporation membrane resealing suggested that the acoustically-mediated calcium influx[85, 91, 107] triggered the trafficking and the fusion of lysosomal vesicles[60, 97] with the plasma membrane (*i.e.*, exocytosis)[108, 109]. Then, they formed a patch across the permeabilized membrane region[110]. Nevertheless, Qin *et al.*, highlighted that the current studies did not provide any spatiotemporal relationship between the acoustically-induced calcium influx and the exocytosis of intracellular vesicles[5]. In addition, if the origin of these vesicles has been mainly demonstrated as lysosomal[60, 97], it cannot be excluded that these intracellular vesicles can arise from other membrane-bound and

calcium-sensitive exocytotic compartments (*e.g.,* early and late endosomes, Golgi apparatus, endoplasmic reticulum)[108].

Lentacker *et al.,* suggested that endocytosis should be directly triggered and physically participating to the resealing of small membrane pores, which are induced by stably oscillating microbubbles[4]. As previously described[60, 97], the exocytosis process for resealing of large membrane pores relies on the exocytosis of lysosomal vesicles. Such exocytosis should release the lysosomal acid sphingomyelinase (ASMases), which converts the sphingomyeline to ceramide[111]. This enzymatic reaction promotes the inward budding and the formation of membrane vesicles, *i.e.,* initiation step of endocytosis[111]. Moreover, Lariccia *et al.,* described that calcium influx could trigger the formation of cholesterol-enriched membrane domains that spontaneously vesiculated to the cytoplasmic side of plasma membrane and caused the formation of endocytic vesicles without involvement of classical endocytic proteins[112, 113]. This process termed massive calcium-activated endocytosis (MEND). However, the roles of sphingomyelinase and calcium-dependent MEND in the *in-vitro* acoustically-mediated delivery of exogenous molecules through the activation of endocytosis is not established today.

3.2. ENDOCYTOSIS

Clathrin- and caveolae-dependent endocytosis processes are the main endocytotic pathways, occurring in the mammalian cells[114, 115]. Several reports described that microbubble-assisted ultrasound promoted the endocytosis-dependent pathways for *in-vitro* delivery of exogenous molecules (**Figure 6**)[63, 89, 96, 116, 117]. However, the molecular and cellular mechanisms responsible for acoustically-mediated endocytosis have not been clearly established. Current investigations suggested that the endocytosis can be caused by the physical interaction between microbubble, ultrasound and cells (*i.e.,* mechanical stimuli) as well as biochemical signals triggered by

mechanical/chemical stimuli or by the formation of membrane pores[4, 5]. In other words, acoustically-mediated endocytosis should be direct or indirect consequences of microbubble-assisted ultrasound.

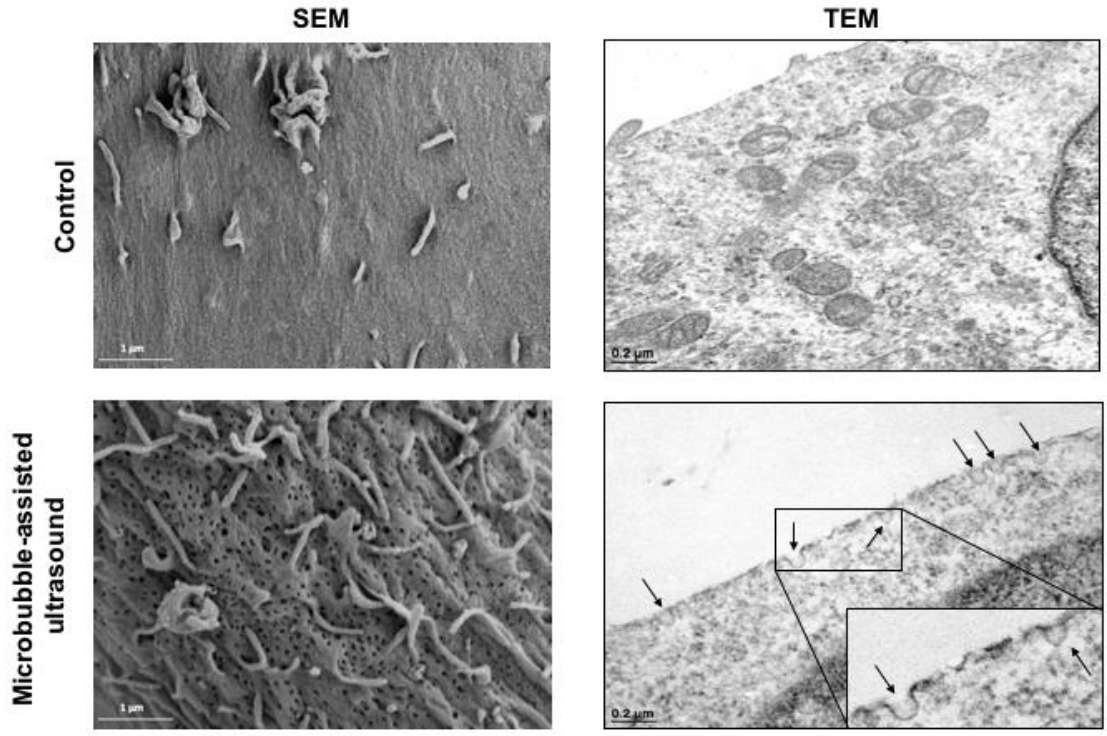

Figure 6. Microbubble-assisted ultrasound stimulates caveolae-dependent endocytosis. Glioblastoma cells were exposed to microbubble-assisted ultrasound (1 MHz, 20% DC, 1 W/cm^2, exposure time of 60 s) and immediately fixed after insonation for subsequent SEM (top view of caveolae-coated pits) and TEM (intracellular view of caveolae-coated pits) imaging (Adapted with permission from Zeghimi *et al.*[63] – Copyright © 2015 IOP Publishing Ltd.).

3.2.1. Endocytosis as a direct consequence of mechanical and/or chemical stimuli

As previously described, mechanical stimuli (*i.e.*, pulling/pushing process, microstreaming, shock waves, microjets) exerted shear stress on the cell plasma membrane, resulting in membrane deformation[37]. Such deformation is thought to play a major role in the initiation of endocytosis pathways[118]. Meijering *et al.*, reported that stably cavitating microbubbles (1 MHz, 0.22 MPa PNP) induced a homogenous distribution of 4.4- and 70- kDa FITC-labelled dextrans through the cytosol of endothelial cells whereas 155- and 500-kDa dextrans were located in distinct intracellular

vesicles[89]. Independently inhibiting clathrin- and caveolae-mediated endocytosis as well as macropinocytosis significantly reduced the intracellular delivery of larger dextrans. These results supported a direct relationship between the macromolecule size and its transmembrane routes[119]. However, recent reports described that microbubble-assisted ultrasound resulted in membrane permeabilization to low molecular weight molecules (< 4 kDa) through the stimulation of endocytosis pathways[63, 116]. Indeed, Derieppe *et al.*, demonstrated that clathrin- and caveolae-dependent endocytosis were recruited for the intracellular uptake of SYTOX Green (600 Da hydrophilic model drug) for several hours when rat glioma cells were exposed to low acoustic pressures (1.4 MHz, 0.2 MPa PNP) in presence of microbubbles[116]. Cells pretreated with chlorpromazine (*i.e.,* inhibitor of clathrin-dependent endocytosis) or genistein (*i.e.,* inhibitor of caveolae-dependent endocytosis) depicted significant decrease in the intracellular delivery of this dye. The lifetime of the endocytosis-dependent pathways is in the order of several tens of minutes to few hours[63, 89, 96, 120]. All together these studies suggested that physical or biological factors other than molecular size might determine the preferred transmembrane pathways for the delivery of exogenous molecules using microbubble-assisted ultrasound.

3.2.2. Endocytosis as an indirect consequence of mechanical and/or chemical stimuli

Cells sense electrical, mechanical and biochemical signals generated from their surrounding environment, which influence their fate[121]. Unlike electrical and biochemical stimuli, mechanical stimuli can propagate without the diffusion of informative molecules (*i.e.,* ions, proteins). Indeed, the mechanical cues are propagated through mechanically stiff structures, flowing, such as cytoskeletal components (*i.e.,* actin filaments, microtubules), causing spatio-temporal changes in cytoskeletal-associated proteins (*e.g.,* filamin; cofilin, myosin, *etc.*) and enzymes related to signal transductions (*e.g.,* monomeric GTPase, phosphoprotein phosphatases, kinases *etc.*)[121]. Previous

investigations suggested that ultrasound-driven microbubbles induced a reversible rearrangement of cytoskeleton[74, 86, 105] but only one reported an association between the membrane deformation and the remodeling of cytoskeleton[106]. Thus, Wang *et al.,* demonstrated that the increase in the acoustic pressures (1 MHz, 0.2-0.4 MPa PNP) or the decrease in the bubble-cell distance caused a significant membrane deformation, which led to enhanced intracellular uptake of propidium iodide and cytoskeleton disassembly[106]. Although the authors described a positive correlation between the membrane permeabilization and the rearrangement of cytoskeleton, they did not investigate whether such membrane deformation and remodeling of cytoskeleton could promote endocytosis-dependent routes.

Membrane mechanosensors such as integrins or mechanosensitive ion channels can sense the mechanical constraints on the cell plasma membrane and convert the mechanical signals into biochemical signals, which result in the stimulation of endocytosis-dependent pathways[121, 122]. The current state of our knowledge indicate that low-intensity pulsed ultrasound (without microbubbles) activated integrin-mediated mechanotransduction pathways (*i.e.*, integrin/FAK/MAPK signaling pathways) in synovial cells (3 MHz, 30 mW/cm^2)[123] and chondrocytes (5 MHz, 14 kPa SAP)[124]. However, both studies did not explore whether the activation of such signaling pathways might induce the stimulation of endocytosis-dependent pathways. Nowadays, there is no evidence that microbubble-assisted ultrasound elicits endocytosis-dependent ways by triggering integrin-mediated mechanotransduction pathways. Further investigations are required to identify the cellular and molecular actors (*e.g.*, microtubules, actin cytoskeletons, integrins, enzymes, calcium signaling, *etc.*) involved in the propagation of mechanical stimuli inside the cell and in the subsequent activation of endocytosis-dependent ways[4, 5].

3.2.3. Endocytosis as an indirect consequence of membrane perforation

As previously described[74, 91, 107], microbubble-assisted ultrasound induced membrane permeability to calcium, increasing thus intracellular calcium level. This calcium influx was responsible for stimulating the endocytosis pathways[4, 5]. Thus, recent electrophysiological studies showed that microbubble-assisted ultrasound (1 MHz, 0.1 and 0.5 MPa PNP) induced a calcium influx through the formation of membrane pores, which led to an activation of BK_{Ca} channels and a subsequent, local membrane hyperpolarization[88, 125]. This membrane hyperpolarization may facilitate the uptake of macromolecules through endocytosis- and macropinocytosis-mediated pathways[88]. Lee *et al.*, reported that microbubble-assisted ultrasound (1 MHz, 2 W/cm^2) enhanced the endocytosis-mediated delivery of PEI:pDNA complexes by increasing PKC-δ related fluid phase endocytosis, which was induced by increasing the intracellular calcium level through the membrane permeabilization to calcium[117]. As reported in section 3.1.2., cells might also trigger the lysosomal ASMase-endocytosis[111] or the MEND[112, 113] for the resealing of membrane pores. However, there is no evidence that both endocytosis processes participate to intracellular delivery of exogenous molecules in the same time as the membrane resealing[4, 5].

3.2.4. Irreversible membrane permeabilization

As formerly indicated, the efficiency of membrane permeabilization is strongly dependent on acoustic parameters and the dose of microbubbles. However, the exposure of cells to harsh ultrasound conditions, including high acoustic pressures (> 1 MPa)[100], long pulse duration (> 1 min)[52] or high dose of microbubbles[93, 100], may induce an irreversible membrane permeabilization through the formation of large and irreparable membrane wounds (> 10 μm)[68, 110]. Karshafian *et al.*, reported that at given acoustic parameters (0.5 MHz, 570 kPa PNP, 120s), increasing Definity® microbubble concentration from 0.067% (v/v) to 13.2% was positively correlated with a

significant and linear decrease in cell viability[93]. In the same way, Qiu *et al.,* described that the cell viability linearly declined when the acoustic pressure (from 0.5 to 3.5 MPa) or the total insonation time (from 10 to 70 s) increased. In agreement with the available literature, the micro-sized membrane wounds are mainly caused by mechanical stress[68, 100]. The number and/or the diameter of such membrane wounds were so high that the permeabilized cells did not have the physiological resources to repair them[63, 110]. All together these data suggested that the optimization of acoustic parameters and dose of microbubbles are required for an efficient and safe delivery of exogenous molecules.

4. PROTOCOLS

4.1. Microbubbles

4.1.1. Microbubble formulation

In most investigations, clinically-approved microbubbles (*e.g.* Definity®, SonoVue®, Sonozoid®) for contrast-enhanced ultrasound imaging have been evaluated for drug delivery[30]. These microbubbles are currently used as an echocontrast agent for ultrasound imaging in order to boost the image contrast[126]. The use of these microbubbles may facilitate the clinical translation of microbubble-assisted ultrasound for drug delivery[24]. These microbubbles are filled with high molecular weight hydrophobic gas (*e.g.,* perfluorocarbon, sulfur hexafluoride) encapsulated by a biocompatible shell (*e.g.,* lipids, proteins, polymers)[30, 127-129]. Based on the shell composition[130], the microbubbles are categorized in two different types: protein- and polymer-shelled microbubbles are thicker and more rigid, while lipid-shelled ones have thinner and more flexible shell. Previous studies reported that soft-shelled microbubbles are more efficient for drug delivery then hard-shelled microbubbles when using same microbubble concentrations and ultrasound settings[93, 131]. Escoffre *et al.,* reported that the exposure of glioblastoma and breast cancer cells to

ultrasound in the presence of lipid-shelled microbubbles (Vevo Micromarker®, BR14®, SonoVue®) induced more efficient delivery of doxorubicin than polylactide-shelled microbubbles[131]. Current investigations showed that these results may be explained by the acoustic pressure-dependent microbubble behavior[29, 32]. The soft-shelled microbubbles oscillate at low acoustic pressures while at higher acoustic pressures, they oscillate more vigorously, leading to their violent collapse and destruction[132]. In contrast, hard-shelled microbubbles are poorly sensitive to low acoustic pressures. At higher acoustic pressures, sonic cracking takes place and induces a small shell defect in hard-shelled microbubbles, thereby releasing of a violent gas stream[132, 133]. This acoustic phenomenon might be involved in the membrane permeabilization through the formation of membrane pores.

As previously reported, microbubble behavior at a given frequency is mainly dependent on its size[29, 32]. Indeed, the resonance frequency of microbubbles decreases as their size increases. Thus, microbubble's acoustic response is stronger around its resonant frequency. Previous studies correlated the stepwise increase in membrane permeabilization to the successive microbubble destructions, which reached the resonant radius of microbubbles[84, 90]. These studies suggested that the design of monodisperse microbubbles responsive to a selected ultrasound settings should be a better option than the current polydisperse microbubbles[30]. Biochemical methods including microfluidic-based[134-136] or ink-jet printing[137] techniques have recently been developed to achieve this goal. In addition, the design of multi-frequency ultrasound sequences (as reported for ultrasound imaging[138]) dedicated for drug delivery would be also a great alternative.

4.1.2. Microbubble/ultrasound/cell interaction

The efficacy of membrane permeabilization could be achieved only when the microbubbles are spatially close to the cell plasma membrane, suggesting the importance of the microbubble-cell

distance (*d*)[139]. Indeed, various studies reported a reversible permeabilization of plasma membrane of cells in suspension[140], in adherence[101] and as well as of *Xenopus oocytes*[95], when the ratio of *d* to the microbubble diameter (D) was less than 0.75. Qin *et al.*, confirmed that microbubble-assisted ultrasound caused localized membrane permeabilization when *d* is less than D and showed that the extent of permeabilization positively correlated with *d*[101]. The efficacy of membrane permeabilization was reported to decay as the inverse-cube power of the nearest microbubble-cell spacing[139]. In view of the importance of *d*/D ratio in the microbubble-assisted ultrasound process, several acoustical and chemical methods were proposed to bring microbubbles in proximity to the targeted biological barriers to reach the critical distance for their permeabilization. Low acoustic pressure (< 0.1 MPa) and long pulse duration (> 1 s) were used to generate directional primary acoustic radiation forces, which push microbubbles towards the surface of biological barriers, thereby improving microbubble-barrier contact[141]. High acoustic pressure pulses (> 0.5 MPa) with short duration (≈ μs) were then transmitted to induce cavitation-mediated permeabilization of biological barriers. Other chemical alternative strategies involved the conjugation of targeting ligands or antibodies onto the microbubble's shell, which then bind to specific overexpressed markers at the surface of targeted cells (*e.g.,* VEGF-R2, PSMA, LHR)[24]. Frinking *et al.,* described the combination of both methods to bring microbubbles near the targeted cells[142]. Indeed, primary radiation forces (38 kPa PNP, 95% DC) induced a sevenfold increase in the binding of VEGF-R2 targeted microbubbles on the endothelial wall in a prostate adenocarcinoma rat model in comparison to non-targeted microbubbles. These strategies have been reported to significantly improve the efficacy of drug delivery.

4.1.3. Coadministration of microbubbles and drugs versus drug-loaded microbubbles

The easiest approach to investigate the biophysical mechanisms involved in acoustically-mediated ultrasound drug delivery is to mix microbubbles and model drugs before their exposure to ultrasound in presence of cells[96, 107, 116]. This approach offers two main advantages[24]: (1) both components can be handled separately until *in-vitro* incubation[89]; (2) instead of mixing both components, two separate administration of these components can also be performed to investigate the post-insonation membrane events (*e.g.*, resealing of membrane pores)[34]. The main limitations of the coadministration approach for *in-vivo* purposes are the different biodistribution and pharmacokinetics of microbubbles and drugs[24].

To overcome these limitations, the microbubble's architecture has been chemically adapted for the loading of drugs[30]. By this way, the microbubbles act not only as cavitation nuclei but also as drug carriers. Lipophilic molecules (*e.g.*, drugs or model drugs) can be loaded into the lipid monolayer of microbubble's shell or dissolved in a hydrophobic cavity (*e.g.*, oil pocket) located between the microbubble's shell and the gas core[30, 33]. Geers *et al.*, designed self-assembled liposome-loaded microbubbles, where drug-loaded nanoparticles (*e.g.*, liposomes) are bound on the microbubble's surface[143]. Nucleic acids (*e.g.*, plasmid DNA, mRNA, siRNA, *etc.*) can also be loaded on microbubbles during the microbubble's assembly or by incubation of nucleic acids with cationic microbubbles[96, 127, 144]. These microbubbles provide additional protection for nucleic acids against serum DNases. As bare microbubbles, drug-loaded microbubbles are able to deliver chemotherapeutic drugs[145, 146] or nucleic acids[11, 147, 148] into the cells through the formation of membrane pores[149]. To the best of our knowledge, no study has been reported that directly compare the acoustic stimuli as well as the molecular and cellular mechanisms of membrane permeabilization induced by the exposure of drug-loaded microbubbles in comparison to bare microbubbles[30].

4.2. Ultrasound devices and settings

Several studies investigated the influence of acoustic parameters (*i.e.,* frequency, acoustic pressure, pulse length, total insonation time, *etc.*) on the microbubble behavior, on the acoustic stimuli (*i.e.*, mechanical, chemical, thermal effects) and on the molecular and cellular mechanisms involved in membrane permeabilization[45, 62, 100]. Among these studies, clinical ultrasound scanners and probes have been used to achieve this goal[150]. If the use of such equipment should facilitate the clinical translation of microbubble-assisted ultrasound for drug delivery, the ultrasound settings are limited for safety reasons and might be not efficient for drug delivery[126]. Hence, laboratory-made and commercial ultrasound devices have been designed to be able to control all acoustic parameters, which can then be used to investigate biophysical mechanisms of membrane permeabilization[23, 48, 117]. In addition, ultrasound transducers used in the literature can be focused[106] or unfocused[109, 120]. It is not straightforward to directly compare the experimental data of most investigations because of a lack of standardized calibration systems concerning the applied acoustic parameters and the heterogeneity in used equipments[107, 151].

As previously described, the choice of frequency to be used depends on the microbubble's size and distribution. The transmission center frequency used for *in-vitro* investigations ranges from 0.25 to 1.5 MHz[60, 68, 95]. The acoustic dose is usually expressed in different units, including acoustic pressure (kPa), acoustic intensity (W/cm$_2$) and MI depending on whether clinical scanner, commercial or home-made ultrasound device is employed. Among *in-vitro* experiments, it is not clearly defined whether acoustic pressure is peak-to-peak pressure, peak negative or positive pressure. In the same way, the acoustic intensity is not obviously stated (*i.e.,* I_{SATA} or I_{SPTA}). Peak negative pressures ranging from 0.010 MPa to 5 MPa have been applied in *in-vitro* studies[52, 60, 87, 133]. Increasing the acoustic pressure enhances transiently the membrane permeability to exogenous

molecules into the cells, but different molecular and cellular mechanisms (*i.e.,* membrane pore *versus* endocytosis) are involved in the membrane permeabilization as a function of acoustic pressure[60, 95, 96]. However, the use of high acoustic pressures (1 MHz, > 0.5 MPa) induces a significant loss of cell viability[52, 60]. In addition, the ultrasound pulse length is another acoustic parameter, which influences the microbubble behavior and thus the efficacy of membrane permeabilization[34, 62, 87, 93].

In most *in-vitro* studies, long ultrasound pulses (milliseconds to seconds) are applied in combination with low acoustic pressures for drug delivery[62, 152]. In opposite, very short ultrasound pulses (few microseconds) might be more effective in combination with high acoustic pressure[93]. Indeed, Fan *et al.,* reported that one single short ultrasound burst but with high acoustic amplitude (1.25 MHz, 0.4 MPa PNP, 10 μs) resulted in higher transfection level (30% *versus* 10%) and higher cell viability (50% *versus* 90%) than one long burst with the same acoustic pressure (1.25 MHz, 0.4 MPa PNP, 10 ms)[153]. This latter led to large and irreversible membrane disruptions, which were responsible for cell death. Total insonation time plays also a major role in drug delivery[4, 24]. During this sonication period, ultrasound pulses are repeatedly emitted at a pulsing interval to activate the microbubbles. Total insonation time from few tens of microseconds to few minutes have been reported in *in-vitro* investigations[24, 151]. However, increasing the total insonation time induces membrane permeabilization at given acoustic pressure, but the use of high insonation time (1 MHz, > 0.5 MPa, > 5 min) induces a significant decrease in cell viability[3, 24]. The number of emitted pulses is also a key parameter for membrane permeabilization. Short burst transmitted at sequentially seem to be more efficient than a single but very long ultrasound burst.

5. CONCLUSION

Local drug delivery using microbubble-assisted ultrasound has a great potential to become a clinically-approved method for improving the efficacy of therapeutic molecules. New advances in high-speed real-time optical imaging have made substantial progress in revealing some of the biophysical causes and, molecular and cellular consequences of this acoustically-mediated drug delivery method over the past ten years. Nevertheless, the lack of detailed knowledge on the origins of stimuli (*e.g.,* mechanical, chemical, thermal stimuli; even their combination) responsible for the membrane permeabilization as well as on the physiological responses (*e.g.,* nature and structure of membrane pores; endocytosis; exocytosis; mechanisms of membrane recovery) might compromise the clinical translation of this ultrasound technology. A consolidation of the current basic knowledge could allow the design of therapeutic microbubbles, dedicated ultrasound sequences and treatment protocols for a controlled, efficient and safe use of this method in the clinics. To achieve this goal, further investigations are required as for example: (1) spatiotemporal relationship between biophysical stimuli and the membrane permeabilization and recovery (2) detailed role of calcium signaling as well as cytoskeleton and its related proteins on both biological processes; (3) involvement of exocytosis and endocytosis in membrane recovery; (4) long-term fate of reversibly permeabilized cells responses.

AUTHOR INFORMATION

Corresponding Authors

Jean-Michel Escoffre, Ph.D., and Ayache Bouakaz, Ph.D., UMR 1253, iBrain, Université de Tours, Inserm, 10 bd Tonnellé, 37032 Tours Cedex 1, France. Tel: +33(0)247366191. Email address: jean-michel.escoffre@univ-tours.fr and ayache.bouakaz@univ-tours.fr.

Funding Sources

This work was supported by the French National Research Agency, Soundelivery Grant – ANR-14-CE17-008, by the National Institute of Cancer, Sonchimio – INCA-DGOS (AB) and Inserm grant (JME).

Notes

The authors declare no competing financial interest.

Biographies

Jean-Michel Escoffre is currently pursuing his research as Senior researcher at the Imaging and Brain Research Unit of the French Institute for Health and Medical Science and Université de Tours (France). He has published over 70 peer-reviewed journal papers, 5 book chapters and coedited 1 book *Therapeutic ultrasound*. His main research interest lies in the fields of drug delivery using microbubble-assisted ultrasound.

Ayache Bouakaz is Deputy Director of Imaging and Brain Research Unit of the French Institute for Health and Medical Science and Université de Tours (France). As Inserm Research Director, he leads the research group "Imaging and Therapeutic Ultrasound". He has published over 130 peer-reviewed journal papers and coedited 2 books *Therapeutic ultrasound* and *Echographie de contraste*. His main research interest lies on the design of ultrasound-based therapeutic methods (sonoporation, ultrasound neurostimulation).

ABBREVIATIONS

US, ultrasound; MBs, Microbubbles; VEGF-R2, vascular endothelial growth factor receptor 2; PSMA, prostate specific membrane antigen; LHR, luteinizing hormone receptor; PNP, peak negative pressure; DC, duty cycle; SEM, Scanning electron microscopy; TEM, Transmission electron microscopy; AFM, Atomic force microscopy; MI, Mechanical index; pDNA, plasmid

DNA; SAP, spatially averaged pressure; MAPK, Mitogen-activated protein kinase; FAK, Focal adhesion kinase; PKC-δ, Protein kinase C – delta; ASMase, acid sphingomyelinase; I_{SATA}, Spatial averaged, temporal averaged intensity; I_{SPTA}, spatial peak, temporal averaged intensity;

REFERENCES

1. Park, K. Controlled drug delivery systems: past forward and future back. *J Control Release* **2014,** *190*, 3-8.
2. Jain, K. K. Current status and future prospects of drug delivery systems. *Methods Mol Biol* **2014,** *1141*, 1-56.
3. Escoffre, J. M.; Bouakaz, A., *Therapeutic ultrasound*. 1 ed.; Springer International Publishing: Switzerland, 2016; p VIII, 465.
4. Lentacker, I.; De Cock, I.; Deckers, R.; De Smedt, S. C.; Moonen, C. T. Understanding ultrasound induced sonoporation: definitions and underlying mechanisms. *Adv Drug Deliv Rev* **2014,** *72*, 49-64.
5. Qin, P.; Han, T.; Yu, A. C. H.; Xu, L. Mechanistic understanding the bioeffects of ultrasound-driven microbubbles to enhance macromolecule delivery. *J Control Release* **2018,** *272*, 169-181.
6. Dimcevski, G.; Kotopoulis, S.; Bjanes, T.; Hoem, D.; Schjott, J.; Gjertsen, B. T.; Biermann, M.; Molven, A.; Sorbye, H.; McCormack, E.; Postema, M.; Gilja, O. H. A human clinical trial using ultrasound and microbubbles to enhance gemcitabine treatment of inoperable pancreatic cancer. *J Control Release* **2016,** *243*, 172-181.
7. Alli, S.; Figueiredo, C. A.; Golbourn, B.; Sabha, N.; Wu, M. Y.; Bondoc, A.; Luck, A.; Coluccia, D.; Maslink, C.; Smith, C.; Wurdak, H.; Hynynen, K.; O'Reilly, M.; Rutka, J. T. Brainstem blood brain barrier disruption using focused ultrasound: A demonstration of feasibility and enhanced doxorubicin delivery. *J Control Release* **2018,** *281*, 29-41.
8. Carpentier, A.; Canney, M.; Vignot, A.; Reina, V.; Beccaria, K.; Horodyckid, C.; Karachi, C.; Leclercq, D.; Lafon, C.; Chapelon, J. Y.; Capelle, L.; Cornu, P.; Sanson, M.; Hoang-Xuan, K.; Delattre, J. Y.; Idbaih, A. Clinical trial of blood-brain barrier disruption by pulsed ultrasound. *Sci Transl Med* **2016,** *8*, (343), 343re2.
9. Devulapally, R.; Lee, T.; Barghava-Shah, A.; Sekar, T. V.; Foygel, K.; Bachawal, S. V.; Willmann, J. K.; Paulmurugan, R. Ultrasound-guided delivery of thymidine kinase-nitroreductase dual therapeutic genes by PEGylated-PLGA/PIE nanoparticles for enhanced triple negative breast cancer therapy. *Nanomedicine (Lond)* **2018,** *13*, (9), 1051-1066.
10. Kopechek, J. A.; Carson, A. R.; McTiernan, C. F.; Chen, X.; Klein, E. C.; Villanueva, F. S. Cardiac Gene Expression Knockdown Using Small Inhibitory RNA-Loaded Microbubbles and Ultrasound. *PLoS One* **2016,** *11*, (7), e0159751.
11. Dewitte, H.; Van Lint, S.; Heirman, C.; Thielemans, K.; De Smedt, S. C.; Breckpot, K.; Lentacker, I. The potential of antigen and TriMix sonoporation using mRNA-loaded microbubbles for ultrasound-triggered cancer immunotherapy. *J Control Release* **2014,** *194*, 28-36.

12. Chen, P. Y.; Hsieh, H. Y.; Huang, C. Y.; Lin, C. Y.; Wei, K. C.; Liu, H. L. Focused ultrasound-induced blood-brain barrier opening to enhance interleukin-12 delivery for brain tumor immunotherapy: a preclinical feasibility study. *J Transl Med* **2015,** *13*, 93.
13. Rodriguez-Frutos, B.; Otero-Ortega, L.; Ramos-Cejudo, J.; Martinez-Sanchez, P.; Barahona-Sanz, I.; Navarro-Hernanz, T.; Gomez-de Frutos Mdel, C.; Diez-Tejedor, E.; Gutierrez-Fernandez, M. Enhanced brain-derived neurotrophic factor delivery by ultrasound and microbubbles promotes white matter repair after stroke. *Biomaterials* **2016,** *100*, 41-52.
14. Liu, H. L.; Hsu, P. H.; Lin, C. Y.; Huang, C. W.; Chai, W. Y.; Chu, P. C.; Huang, C. Y.; Chen, P. Y.; Yang, L. Y.; Kuo, J. S.; Wei, K. C. Focused Ultrasound Enhances Central Nervous System Delivery of Bevacizumab for Malignant Glioma Treatment. *Radiology* **2016,** *281*, (1), 99-108.
15. Kobus, T.; Zervantonakis, I. K.; Zhang, Y.; McDannold, N. J. Growth inhibition in a brain metastasis model by antibody delivery using focused ultrasound-mediated blood-brain barrier disruption. *J Control Release* **2016,** *238*, 281-288.
16. Alkins, R.; Burgess, A.; Kerbel, R.; Wels, W. S.; Hynynen, K. Early treatment of HER2-amplified brain tumors with targeted NK-92 cells and focused ultrasound improves survival. *Neuro Oncol* **2016,** *18*, (7), 974-81.
17. Burgess, A.; Ayala-Grosso, C. A.; Ganguly, M.; Jordao, J. F.; Aubert, I.; Hynynen, K. Targeted delivery of neural stem cells to the brain using MRI-guided focused ultrasound to disrupt the blood-brain barrier. *PLoS One* **2011,** *6*, (11), e27877.
18. Sanches, P. G.; Grull, H.; Steinbach, O. C. See, reach, treat: ultrasound-triggered image-guided drug delivery. *Ther Deliv* **2011,** *2*, (7), 919-34.
19. Song, S.; Guo, G.; Jiang, Z.; Jin, Y.; Zhang, Z.; Sun, K.; Dou, H. Self-Assembled Fe3O4/Polymer Hybrid Microbubble with MRI/Ultrasound Dual-Imaging Enhancement. *Langmuir* **2016,** *30*, (35), 10557-10561.
20. Teraphongphom, N.; Chhour, P.; Eisenbrey, J. R.; Naha, P. C.; Witschey, W. R. T.; Opasanont, B.; Jablonowski, L.; Cormode, D. P.; Wheatley, M. A. Nanoparticle Loaded Polymeric Microbubbles as Contrast Agents for Multimodal Imaging. *Langmuir* **2015,** *31*, (43), 11858-11867.
21. Xu, B.; Dou, H.; Tao, K.; Sun, K.; Ding, J.; Shi, W.; Guo, X.; Li, J.; Zhang, D.; Sun, K. "Two-in-One" Fabrication of Fe3O4/MePEG-PLA Composite Nanocapsules as a Potential Ultrasonic/MRI Dual Contrast Agent. *Langmuir* **2011,** *27*, (19), 12134-12142.
22. Liao, A. H.; Ma, W. C.; Wang, C. H.; Yeh, M. K. Penetration depth, concentration and efficiency of transdermal alpha-arbutin delivery after ultrasound treatment with albumin-shelled microbubbles in mice. *Drug Deliv* **2016,** *23*, (7), 2173-2182.
23. Escoffre, J. M.; Novell, A.; Serriere, S.; Lecomte, T.; Bouakaz, A. Irinotecan delivery by microbubble-assisted ultrasound: in vitro validation and a pilot preclinical study. *Mol Pharm* **2013,** *10*, (7), 2667-75.
24. Lammertink, B. H.; Bos, C.; Deckers, R.; Storm, G.; Moonen, C. T.; Escoffre, J. M. Sonochemotherapy: from bench to bedside. *Front Pharmacol* **2015,** *6*, 138.
25. Lipsman, N.; Meng, Y.; Bethune, A. J.; Huang, Y.; Lam, B.; Masellis, M.; Herrmann, N.; Heyn, C.; Aubert, I.; Boutet, A.; Smith, G. S.; Hynynen, K.; Black, S. E. Blood-brain barrier opening in Alzheimer's disease using MR-guided focused ultrasound. *Nat Commun* **2018,** *9*, (1), 2336.

26. Auboire, L.; Sennoga, C. A.; Hyvelin, J. M.; Ossant, F.; Escoffre, J. M.; Tranquart, F.; Bouakaz, A. Microbubbles combined with ultrasound therapy in ischemic stroke: A systematic review of in-vivo preclinical studies. *PLoS One* **2018,** *13*, (2), e0191788.
27. Castle, J.; Feinstein, S. B. Drug and Gene Delivery using Sonoporation for Cardiovascular Disease. *Adv Exp Med Biol* **2016,** *880*, 331-8.
28. Leong-Poi, H.; Kuliszewski, M. A.; Lekas, M.; Sibbald, M.; Teichert-Kuliszewska, K.; Klibanov, A. L.; Stewart, D. J.; Lindner, J. R. Therapeutic arteriogenesis by ultrasound-mediated VEGF165 plasmid gene delivery to chronically ischemic skeletal muscle. *Circ Res* **2007,** *101*, (3), 295-303.
29. Shpak, O.; Verweij, M.; de Jong, N.; Versluis, M. Droplets, Bubbles and Ultrasound Interactions. *Adv Exp Med Biol* **2016,** *880*, 157-74.
30. Bettinger, T.; Tranquart, F. Design of Microbubbles for Gene/Drug Delivery. *Adv Exp Med Biol* **2016,** *880*, 191-204.
31. Martin, K. H.; Dayton, P. A. Current status and prospects for microbubbles in ultrasound theranostics. *Wiley Interdiscip Rev Nanomed Nanobiotechnol* **2013,** *5*, (4), 329-45.
32. Kooiman, K.; Vos, H. J.; Versluis, M.; de Jong, N. Acoustic behavior of microbubbles and implications for drug delivery. *Adv Drug Deliv Rev* **2014,** *72*, 28-48.
33. Sennoga, C. A.; Kanbar, E.; Auboire, L.; Dujardin, P. A.; Fouan, D.; Escoffre, J. M.; Bouakaz, A. Microbubble-mediated ultrasound drug-delivery and therapeutic monitoring. *Expert Opin Drug Deliv* **2017,** *14*, (9), 1031-1043.
34. van Wamel, A.; Kooiman, K.; Harteveld, M.; Emmer, M.; ten Cate, F. J.; Versluis, M.; de Jong, N. Vibrating microbubbles poking individual cells: drug transfer into cells via sonoporation. *J Control Release* **2006,** *112*, (2), 149-55.
35. Kooiman, K.; Foppen-Harteveld, M.; van der Steen, A. F.; de Jong, N. Sonoporation of endothelial cells by vibrating targeted microbubbles. *J Control Release* **2011,** *154*, (1), 35-41.
36. van Rooij, T.; Skachkov, I.; Beekers, I.; Lattwein, K. R.; Voorneveld, J. D.; Kokhuis, T. J. A.; Bera, D.; Luan, Y.; van der Steen, A. F. W.; de Jong, N.; Kooiman, K. Viability of endothelial cells after ultrasound-mediated sonoporation: Influence of targeting, oscillation, and displacement of microbubbles. *J Control Release* **2016,** *238*, 197-211.
37. VanBavel, E. Effects of shear stress on endothelial cells: possible relevance for ultrasound applications. *Prog Biophys Mol Biol* **2007,** *93*, (1-3), 374-83.
38. Wu, J.; Nyborg, W. L. Ultrasound, cavitation bubbles and their interaction with cells. *Adv Drug Deliv Rev* **2008,** *60*, (10), 1103-16.
39. Collis, J.; Manasseh, R.; Liovic, P.; Tho, P.; Ooi, A.; Petkovic-Duran, K.; Zhu, Y. Cavitation microstreaming and stress fields created by microbubbles. *Ultrasonics* **2010,** *50*, (2), 273-9.
40. Wu, J. Theoretical study on shear stress generated by microstreaming surrounding contrast agents attached to living cells. *Ultrasound Med Biol* **2002,** *28*, (1), 125-9.
41. Doinikov, A. A.; Bouakaz, A. Theoretical investigation of shear stress generated by a contrast microbubble on the cell membrane as a mechanism for sonoporation. *J Acoust Soc Am* **2010,** *128*, (1), 11-9.
42. Chen, C.; Gu, Y.; Tu, J.; Guo, X.; Zhang, D. Microbubble oscillating in a microvessel filled with viscous fluid: A finite element modeling study. *Ultrasonics* **2016,** *66*, 54-64.
43. Helfield, B.; Chen, X.; Watkins, S. C.; Villanueva, F. S. Biophysical insight into mechanisms of sonoporation. *Proc Natl Acad Sci U S A* **2016,** *113*, (36), 9983-9.

44. Marmottant, P.; Hilgenfeldt, S. Controlled vesicle deformation and lysis by single oscillating bubbles. *Nature* **2003,** *423*, (6936), 153-6.
45. Qiu, Y.; Zhang, C.; Tu, J.; Zhang, D. Microbubble-induced sonoporation involved in ultrasound-mediated DNA transfection in vitro at low acoustic pressures. *J Biomech* **2012,** *45*, (8), 1339-45.
46. Nejad, S. M.; Hosseini, H.; Akiyama, H.; Tachibana, K. Reparable Cell Sonoporation in Suspension: Theranostic Potential of Microbubble. *Theranostics* **2016,** *6*, (4), 446-55.
47. Ibsen, S.; Benchimol, M.; Esener, S. Fluorescent microscope system to monitor real-time interactions between focused ultrasound, echogenic drug delivery vehicles, and live cell membranes. *Ultrasonics* **2013,** *53*, (1), 178-84.
48. Luan, Y.; Lajoinie, G.; Gelderblom, E.; Skachkov, I.; van der Steen, A. F.; Vos, H. J.; Versluis, M.; De Jong, N. Lipid shedding from single oscillating microbubbles. *Ultrasound Med Biol* **2014,** *40*, (8), 1834-46.
49. Doinikov, A. A.; Bouakaz, A. Acoustic microstreaming around an encapsulated particle. *J Acoust Soc Am* **2010,** *127*, (3), 1218-27.
50. Forbes, M. M.; O'Brien, W. D., Jr. Development of a theoretical model describing sonoporation activity of cells exposed to ultrasound in the presence of contrast agents. *J Acoust Soc Am* **2012,** *131*, (4), 2723-9.
51. Postema, M.; van Wamel, A.; Lancee, C. T.; de Jong, N. Ultrasound-induced encapsulated microbubble phenomena. *Ultrasound Med Biol* **2004,** *30*, (6), 827-40.
52. Qiu, Y.; Luo, Y.; Zhang, Y.; Cui, W.; Zhang, D.; Wu, J.; Zhang, J.; Tu, J. The correlation between acoustic cavitation and sonoporation involved in ultrasound-mediated DNA transfection with polyethylenimine (PEI) in vitro. *J Control Release* **2010,** *145*, (1), 40-8.
53. Kodama, T.; Tomita, Y.; Koshiyama, K.; Blomley, M. J. Transfection effect of microbubbles on cells in superposed ultrasound waves and behavior of cavitation bubble. *Ultrasound Med Biol* **2006,** *32*, (6), 905-14.
54. Steinbach, P.; Hofstadter, F.; Nicolai, H.; Rossler, W.; Wieland, W. In vitro investigations on cellular damage induced by high energy shock waves. *Ultrasound Med Biol* **1992,** *18*, (8), 691-9.
55. Goni, F. M. The basic structure and dynamics of cell membranes: an update of the Singer-Nicolson model. *Biochim Biophys Acta* **2014,** *1838*, (6), 1467-76.
56. Koshiyama, K.; Kodama, T.; Yano, T.; Fujikawa, S. Structural change in lipid bilayers and water penetration induced by shock waves: molecular dynamics simulations. *Biophys J* **2006,** *91*, (6), 2198-205.
57. Koshiyama, K.; Kodama, T.; Yano, T.; Fujikawa, S. Molecular dynamics simulation of structural changes of lipid bilayers induced by shock waves: Effects of incident angles. *Biochim Biophys Acta* **2008,** *1778*, (6), 1423-8.
58. Koshiyama, K.; Yano, T.; Kodama, T. Self-organization of a stable pore structure in a phospholipid bilayer. *Phys Rev Lett* **2010,** *105*, (1), 018105.
59. Mehier-Humbert, S.; Bettinger, T.; Yan, F.; Guy, R. H. Plasma membrane poration induced by ultrasound exposure: implication for drug delivery. *J Control Release* **2005,** *104*, (1), 213-22.
60. Yang, F.; Gu, N.; Chen, D.; Xi, X.; Zhang, D.; Li, Y.; Wu, J. Experimental study on cell self-sealing during sonoporation. *J Control Release* **2008,** *131*, (3), 205-10.

61. Zhao, Y. Z.; Luo, Y. K.; Lu, C. T.; Xu, J. F.; Tang, J.; Zhang, M.; Zhang, Y.; Liang, H. D. Phospholipids-based microbubbles sonoporation pore size and reseal of cell membrane cultured in vitro. *J Drug Target* **2008,** *16*, (1), 18-25.
62. Duvshani-Eshet, M.; Machluf, M. Therapeutic ultrasound optimization for gene delivery: a key factor achieving nuclear DNA localization. *J Control Release* **2005,** *108*, (2-3), 513-28.
63. Zeghimi, A.; Escoffre, J. M.; Bouakaz, A. Role of endocytosis in sonoporation-mediated membrane permeabilization and uptake of small molecules: a electron microscopy study. *Phys Biol* **2015,** *12*, (6), 066007.
64. Postema, M.; van Wamel, A.; ten Cate, F. J.; de Jong, N. High-speed photography during ultrasound illustrates potential therapeutic applications of microbubbles. *Med Phys* **2005,** *32*, (12), 3707-11.
65. Ohl, C. D.; Arora, M.; Ikink, R.; de Jong, N.; Versluis, M.; Delius, M.; Lohse, D. Sonoporation from jetting cavitation bubbles. *Biophys J* **2006,** *91*, (11), 4285-95.
66. Cook, S. S. Erosion by water-hammer. *Proc Roy Soc London A* **1928**, (119), 1131-1134.
67. Prentice, P.; Cuschieri, A.; Dholakia, K.; Prausnitz, M.; Campbell, P. Membrane disruption by optically controlled microbubble cavitation. *Nature Phys* **2005,** *1*, 107-110.
68. Kudo, N.; Okada, K.; Yamamoto, K. Sonoporation by single-shot pulsed ultrasound with microbubbles adjacent to cells. *Biophys J* **2009,** *96*, (12), 4866-76.
69. Oswald, M. C. W.; Garnham, N.; Sweeney, S. T.; Landgraf, M. Regulation of neuronal development and function by ROS. *FEBS Lett* **2018,** *592*, (5), 679-691.
70. Ishimoto, Y.; Tanaka, T.; Yoshida, Y.; Inagi, R. Physiological and Pathophysiological Role of Reactive Oxygen Species and Reactive Nitrogen Species in the Kidney. *Clin Exp Pharmacol Physiol* **2018**.
71. Cordeiro, R. M. Reactive oxygen species at phospholipid bilayers: distribution, mobility and permeation. *Biochim Biophys Acta* **2014,** *1838*, (1 Pt B), 438-44.
72. Wei, D. H.; Zhang, X. L.; Wang, R.; Zeng, J. F.; Zhang, K.; Yang, J.; Li, S.; Lin, X. L.; Jiang, Z. S.; Wang, G. X.; Wang, Z. Oxidized lipoprotein(a) increases endothelial cell monolayer permeability via ROS generation. *Lipids* **2013,** *48*, (6), 579-86.
73. Juffermans, L. J.; Dijkmans, P. A.; Musters, R. J.; Visser, C. A.; Kamp, O. Transient permeabilization of cell membranes by ultrasound-exposed microbubbles is related to formation of hydrogen peroxide. *Am J Physiol Heart Circ Physiol* **2006,** *291*, (4), H1595-601.
74. Juffermans, L. J.; van Dijk, A.; Jongenelen, C. A.; Drukarch, B.; Reijerkerk, A.; de Vries, H. E.; Kamp, O.; Musters, R. J. Ultrasound and microbubble-induced intra- and intercellular bioeffects in primary endothelial cells. *Ultrasound Med Biol* **2009,** *35*, (11), 1917-27.
75. Leung, K. S.; Chen, X.; Zhong, W.; Yu, A. C.; Lee, C. Y. Microbubble-mediated sonoporation amplified lipid peroxidation of Jurkat cells. *Chem Phys Lipids* **2014,** *180*, 53-60.
76. Wong-Ekkabut, J.; Xu, Z.; Triampo, W.; Tang, I. M.; Tieleman, D. P.; Monticelli, L. Effect of lipid peroxidation on the properties of lipid bilayers: a molecular dynamics study. *Biophys J* **2007,** *93*, (12), 4225-36.
77. Lionetti, V.; Fittipaldi, A.; Agostini, S.; Giacca, M.; Recchia, F. A.; Picano, E. Enhanced caveolae-mediated endocytosis by diagnostic ultrasound in vitro. *Ultrasound Med Biol* **2009,** *35*, (1), 136-43.
78. Escoffre, J. M.; Campomanes, P.; Tarek, M.; Bouakaz, A., New insights in the role of ROS in mechanisms of sonoporation-mediated gene delivery. In *The 23rd European Symposium on Ultrasound Contrast Imaging*, de Jong, N.; ten Cate, F. J.; Vos, R.; Kooiman, K.; Schinkel, A., Eds. Erasmus MC Rotterdam: Rotterdam, The Netherlands, 2018; 'Vol.' 23, pp 41-43.

79. Wu, J. Temperature rise generated by ultrasound in the presence of contrast agent. *Ultrasound Med Biol* **1998,** *24*, (2), 267-74.
80. Lawaczeck, R.; Kainosho, M.; Chan, S. I. The formation and annealing of structural defects in lipid bilayer vesicles. *Biochim Biophys Acta* **1976,** *443*, (3), 313-30.
81. Tsong, T. Y. Effect of phase transition on the kinetics of dye transport in phospholipid bilater structures. *Biochemistry* **1975,** *14*, (25), 5409-14.
82. Antonov, V. F.; Petrov, V. V.; Molnar, A. A.; Predvoditelev, D. A.; Ivanov, A. S. The appearance of single-ion channels in unmodified lipid bilayer membranes at the phase transition temperature. *Nature* **1980,** *283*, (5747), 585-6.
83. Boheim, G.; Hanke, W.; Eibl, H. Lipid phase transition in planar bilayer membrane and its effect on carrier- and pore-mediated ion transport. *Proc Natl Acad Sci U S A* **1980,** *77*, (6), 3403-7.
84. Fan, Z.; Liu, H.; Mayer, M.; Deng, C. X. Spatiotemporally controlled single cell sonoporation. *Proc Natl Acad Sci U S A* **2012,** *109*, (41), 16486-91.
85. Hu, Y.; Wan, J. M.; Yu, A. C. Membrane perforation and recovery dynamics in microbubble-mediated sonoporation. *Ultrasound Med Biol* **2013,** *39*, (12), 2393-405.
86. Fan, Z.; Chen, D.; Deng, C. X. Characterization of the dynamic activities of a population of microbubbles driven by pulsed ultrasound exposure in sonoporation. *Ultrasound Med Biol* **2014,** *40*, (6), 1260-72.
87. van Wamel, A.; Bouakaz, A.; Versluis, M.; de Jong, N. Micromanipulation of endothelial cells: ultrasound-microbubble-cell interaction. *Ultrasound Med Biol* **2004,** *30*, (9), 1255-8.
88. Juffermans, L. J.; Kamp, O.; Dijkmans, P. A.; Visser, C. A.; Musters, R. J. Low-intensity ultrasound-exposed microbubbles provoke local hyperpolarization of the cell membrane via activation of BK(Ca) channels. *Ultrasound Med Biol* **2008,** *34*, (3), 502-8.
89. Meijering, B. D.; Juffermans, L. J.; van Wamel, A.; Henning, R. H.; Zuhorn, I. S.; Emmer, M.; Versteilen, A. M.; Paulus, W. J.; van Gilst, W. H.; Kooiman, K.; de Jong, N.; Musters, R. J.; Deelman, L. E.; Kamp, O. Ultrasound and microbubble-targeted delivery of macromolecules is regulated by induction of endocytosis and pore formation. *Circ Res* **2009,** *104*, (5), 679-87.
90. Deng, C. X.; Sieling, F.; Pan, H.; Cui, J. Ultrasound-induced cell membrane porosity. *Ultrasound Med Biol* **2004,** *30*, (4), 519-26.
91. Fan, Z.; Kumon, R. E.; Park, J.; Deng, C. X. Intracellular delivery and calcium transients generated in sonoporation facilitated by microbubbles. *J Control Release* **2010,** *142*, (1), 31-9.
92. Afadzi, M.; Strand, S. P.; Nilssen, E. A.; Masoy, S. E.; Johansen, T. F.; Hansen, R.; Angelsen, B. A.; de, L. D. C. Mechanisms of the ultrasound-mediated intracellular delivery of liposomes and dextrans. *IEEE Trans Ultrason Ferroelectr Freq Control* **2013,** *60*, (1), 21-33.
93. Karshafian, R.; Samac, S.; Bevan, P. D.; Burns, P. N. Microbubble mediated sonoporation of cells in suspension: clonogenic viability and influence of molecular size on uptake. *Ultrasonics* **2010,** *50*, (7), 691-7.
94. Duvshani-Eshet, M.; Baruch, L.; Kesselman, E.; Shimoni, E.; Machluf, M. Therapeutic ultrasound-mediated DNA to cell and nucleus: bioeffects revealed by confocal and atomic force microscopy. *Gene Ther* **2006,** *13*, (2), 163-72.
95. Zhou, Y.; Yang, K.; Cui, J.; Ye, J. Y.; Deng, C. X. Controlled permeation of cell membrane by single bubble acoustic cavitation. *J Control Release* **2012,** *157*, (1), 103-11.

96. De Cock, I.; Zagato, E.; Braeckmans, K.; Luan, Y.; de Jong, N.; De Smedt, S. C.; Lentacker, I. Ultrasound and microbubble mediated drug delivery: acoustic pressure as determinant for uptake via membrane pores or endocytosis. *J Control Release* **2015,** *197*, 20-8.
97. Zhou, Y.; Shi, J.; Cui, J.; Deng, C. X. Effects of extracellular calcium on cell membrane resealing in sonoporation. *J Control Release* **2008,** *126*, (1), 34-43.
98. Zhou, Y.; Kumon, R. E.; Cui, J.; Deng, C. X. The size of sonoporation pores on the cell membrane. *Ultrasound Med Biol* **2009,** *35*, (10), 1756-60.
99. Qin, P.; Xu, L.; Hu, Y.; Zhong, W.; Cai, P.; Du, L.; Jin, L.; Yu, A. C. Sonoporation-induced depolarization of plasma membrane potential: analysis of heterogeneous impact. *Ultrasound Med Biol* **2014,** *40*, (5), 979-89.
100. Lai, C. Y.; Wu, C. H.; Chen, C. C.; Li, P. C. Quantitative relations of acoustic inertial cavitation with sonoporation and cell viability. *Ultrasound Med Biol* **2006,** *32*, (12), 1931-41.
101. Qin, P.; Xu, L.; Han, T.; Du, L.; Yu, A. C. Effect of non-acoustic parameters on heterogeneous sonoporation mediated by single-pulse ultrasound and microbubbles. *Ultrason Sonochem* **2016,** *31*, 107-15.
102. Zhou, Y.; Cui, J.; Deng, C. X. Dynamics of sonoporation correlated with acoustic cavitation activities. *Biophys J* **2008,** *94*, (7), L51-3.
103. Draeger, A.; Monastyrskaya, K.; Babiychuk, E. B. Plasma membrane repair and cellular damage control: the annexin survival kit. *Biochem Pharmacol* **2011,** *81*, (6), 703-12.
104. Andrews, N. W.; Almeida, P. E.; Corrotte, M. Damage control: cellular mechanisms of plasma membrane repair. *Trends Cell Biol* **2014,** *24*, (12), 734-742.
105. Chen, X.; Leow, R. S.; Hu, Y.; Wan, J. M.; Yu, A. C. Single-site sonoporation disrupts actin cytoskeleton organization. *J R Soc Interface* **2014,** *11*, (95), 20140071.
106. Wang, M.; Zhang, Y.; Cai, C.; Tu, J.; Guo, X.; Zhang, D. Sonoporation-induced cell membrane permeabilization and cytoskeleton disassembly at varied acoustic and microbubble-cell parameters. *Sci Rep* **2018,** *8*, (1), 3885.
107. Escoffre, J. M.; Derieppe, M.; Lammertink, B.; Bos, C.; Moonen, C. Microbubble-Assisted Ultrasound-Induced Transient Phosphatidylserine Translocation. *Ultrasound Med Biol* **2017,** *43*, (4), 838-851.
108. Hussein, F.; Antonescu, C.; Karshafian, R. Ultrasound and microbubble induced release from intracellular compartments. *BMC Biotechnol* **2017,** *17*, (1), 45.
109. Yuana, Y.; Jiang, L.; Lammertink, B. H. A.; Vader, P.; Deckers, R.; Bos, C.; Schiffelers, R. M.; Moonen, C. Microbubbles-assisted ultrasound triggers the release of extracellular vesicles. *Int J Mol Sci* **2017,** *18*, (1610), 1-12.
110. Schlicher, R. K.; Hutcheson, J. D.; Radhakrishna, H.; Apkarian, R. P.; Prausnitz, M. R. Changes in cell morphology due to plasma membrane wounding by acoustic cavitation. *Ultrasound Med Biol* **2010,** *36*, (4), 677-92.
111. Andrews, N. W.; Corrotte, M.; Castro-Gomes, T. Above the fray: Surface remodeling by secreted lysosomal enzymes leads to endocytosis-mediated plasma membrane repair. *Semin Cell Dev Biol* **2015,** *45*, 10-7.
112. Fine, M.; Llaguno, M. C.; Lariccia, V.; Lin, M. J.; Yaradanakul, A.; Hilgemann, D. W. Massive endocytosis driven by lipidic forces originating in the outer plasmalemmal monolayer: a new approach to membrane recycling and lipid domains. *J Gen Physiol* **2011,** *137*, (2), 137-54.
113. Lariccia, V.; Fine, M.; Magi, S.; Lin, M. J.; Yaradanakul, A.; Llaguno, M. C.; Hilgemann, D. W. Massive calcium-activated endocytosis without involvement of classical endocytic proteins. *J Gen Physiol* **2011,** *137*, (1), 111-32.

114. McMahon, H. T.; Boucrot, E. Molecular mechanism and physiological functions of clathrin-mediated endocytosis. *Nat Rev Mol Cell Biol* **2011,** *12*, (8), 517-33.
115. Lajoie, P.; Nabi, I. R. Lipid rafts, caveolae, and their endocytosis. *Int Rev Cell Mol Biol* **2010,** *282*, (135-163).
116. Derieppe, M.; Rojek, K.; Escoffre, J. M.; de Senneville, B. D.; Moonen, C.; Bos, C. Recruitment of endocytosis in sonopermeabilization-mediated drug delivery: a real-time study. *Phys Biol* **2015,** *12*, (4), 046010.
117. Lee, J. L.; Lo, C. W.; Inserra, C.; Bera, J. C.; Chen, W. S. Ultrasound enhanced PEI-mediated gene delivery through increasing the intracellular calcium level and PKC-delta protein expression. *Pharm Res* **2014,** *31*, (9), 2354-66.
118. Apodaca, G. Modulation of membrane traffic by mechanical stimuli. *Am J Physiol Ren Physiol* **2002,** *282*, F179-190.
119. Rejman, J.; Oberle, V.; Zuhorn, I. S.; Hoekstra, D. Size-dependent internalization of particles via the pathways of clathrin- and caveolae-mediated endocytosis. *Biochem J* **2004,** *377*, (Pt 1), 159-69.
120. Fekri, F.; Delos Santos, R. C.; Karshafian, R.; Antonescu, C. N. Ultrasound Microbubble Treatment Enhances Clathrin-Mediated Endocytosis and Fluid-Phase Uptake through Distinct Mechanisms. *PLoS One* **2016,** *11*, (6), e0156754.
121. Yusko, E. C.; Asbury, C. L. Force is a signal that cells cannot ignore. *Mol Biol Cell* **2017,** *25*, (23), 3717-3725.
122. Furthauer, M.; Smythe, E. Systems dynamics in endocytosis. *Traffic* **2014,** *15*, (3), 338-46.
123. Sato, M.; Nagata, K.; Kuroda, S.; Horiuchi, S.; Nakamura, T.; Karima, M.; Inubushi, T.; Tanaka, E. Low-intensity pulsed ultrasound activates integrin-mediated mechanotransduction pathway in synovial cells. *Ann Biomed Eng* **2014,** *42*, (10), 2156-63.
124. Whitney, N. P.; Lamb, A. C.; Louw, T. M.; Subramanian, A. Integrin-mediated mechanotransduction pathway of low-intensity continuous ultrasound in human chondrocytes. *Ultrasound Med Biol* **2012,** *38*, (10), 1734-43.
125. Tran, T. A.; Roger, S.; Le Guennec, J. Y.; Tranquart, F.; Bouakaz, A. Effect of ultrasound-activated microbubbles on the cell electrophysiological properties. *Ultrasound Med Biol* **2007,** *33*, (1), 158-63.
126. Szabo, T. L., *Diagnostic ultrasond imaging: Inside out*. 2nd Edition ed.; Academic Press: 2013.
127. Lentacker, I.; de Geest, B. G.; Vandenbrouke, R. E.; Peeters, L.; Demeester, J.; De Smedt, S. C.; Sanders, N. N. Ultrasound-Responsive Polymer-Coated Microbubbles That Bind and Protect DNA. *Langmuir* **2006,** *22*, (17), 7273-7278.
128. Rossi, S.; Waton, G.; Krafft, M. P. Phospholipid-Coated Gas Bubble Engineering: Key Parameters for Size and Stability Control, as Determined by an Acoustical Method. *Langmuir* **2010,** *26*, (3), 1649-1655.
129. Tsao, N. H.; Hall, E. A. H. Enzyme-Degradable Hybrid Polymer/Silica Microbubbles as Ultrasound Contrast Agents. *Langmuir* **2016,** *32*, (25), 6534-6543.
130. Abou-Saleh, R. H.; Swain, M.; Evans, S. D.; Thomson, N. H. Poly(ethylene glycol) Lipid-Shelled Microbubbles: Abundance, Stability, and Mechanical Properties. *Langmuir* **2014,** *30*, (19), 5557-5563.
131. Escoffre, J. M.; Piron, J.; Novell, A.; Bouakaz, A. Doxorubicin delivery into tumor cells with ultrasound and microbubbles. *Mol Pharm* **2011,** *8*, (3), 799-806.

132. Bloch, S. H.; Wan, M.; Dayton, P. A.; Ferrara, K. W. Optical observations of lipid- and polymer-shelled ultrasound microbubble contrast agents. *Applied Physics Letters* **2004,** *84*, (4), 631-633.
133. Bouakaz, A.; Versluis, M.; de Jong, N. High-speed optical observations of contrast agent destruction. *Ultrasound Med Biol* **2005,** *31*, (3), 391-9.
134. Hettiarachchi, K.; Zhang, S.; Feingold, S.; Lee, A. P.; Dayton, P. A. Controllable microfluidic synthesis of multiphase drug-carrying lipospheres for site-targeted therapy. *Biotechnol Prog* **2009,** *25*, (4), 938-45.
135. Talu, E.; Hettiarachchi, K.; Powell, R. L.; Lee, A. P.; Dayton, P. A.; Longo, M. L. Maintaining Monodispersity in a Microbubble Population Formed by Flow-Focusing. *Langmuir* **2008,** *24*, (5), 1745-1749.
136. Angilè, F. E.; Vargo, K. B.; Sehgal, C. M.; Hammer, D. A.; Lee, D. Recombinant Protein-Stabilized Monodisperse Microbubbles with Tunable Size Using a Valve-Based Microfluidic Device. *Langmuir* **2014,** *30*, (42), 12610-12618.
137. Bohmer, M. R.; Steenbakkers, J. A.; Chlon, C. Monodisperse polymeric particles prepared by ink-jet printing: double emulsions, hydrogels and polymer mixtures. *Colloids Surf B Biointerfaces* **2010,** *79*, (1), 47-52.
138. Novell, A.; Sennoga, C. A.; Escoffre, J. M.; Chaline, J.; Bouakaz, A. Evaluation of chirp reversal power modulation sequence for contrast agent imaging. *Phys Med Biol* **2014,** *59*, (17), 5101-17.
139. Ward, M.; Wu, J.; Chiu, J. F. Experimental study of the effects of Optison concentration on sonoporation in vitro. *Ultrasound Med Biol* **2000,** *26*, (7), 1169-75.
140. Gac, S. L.; Zwaan, E.; van den Berg, A.; Ohl, C. D. Sonoporation of suspension cells with a single cavitation bubble in a microfluidic confinement. *Lab Chip* **2007,** *7*, (12), 1666-72.
141. Shortencarier, M. J.; Dayton, P. A.; Bloch, S. H.; Schumann, P. A.; Matsunaga, T. O.; Ferrara, K. W. A method for radiation-force localized drug delivery using gas-filled lipospheres. *IEEE Trans Ultrason Ferroelectr Freq Control* **2004,** *51*, (7), 822-31.
142. Frinking, P. J.; Tardy, I.; Theraulaz, M.; Arditi, M.; Powers, J.; Pochon, S.; Tranquart, F. Effects of acoustic radiation force on the binding efficiency of BR55, a VEGFR2-specific ultrasound contrast agent. *Ultrasound Med Biol* **2012,** *38*, (8), 1460-9.
143. Geers, B.; Lentacker, I.; Sanders, N. N.; Demeester, J.; Meairs, S.; De Smedt, S. C. Self-assembled liposome-loaded microbubbles: The missing link for safe and efficient ultrasound triggered drug-delivery. *J Control Release* **2011,** *152*, (2), 249-56.
144. Delalande, A.; Bastié, C.; Pigeon, L.; Manta, S.; Lebertre, M.; Mignet, N.; Midoux, P.; Pichon, C. Cationic gas-filled microbubbles for ultrasound-based nucleic acids delivery. *J Control Release* **2017,** *37*, (6), BSR20160619.
145. Escoffre, J. M.; Mannaris, C.; Geers, B.; Novell, A.; Lentacker, I.; Averkiou, M.; Bouakaz, A. Doxorubicin liposome-loaded microbubbles for contrast imaging and ultrasound-triggered drug delivery. *IEEE Trans Ultrason Ferroelectr Freq Control* **2013,** *60*, (1), 78-87.
146. Eisenbrey, J. R.; Soulen, M. C.; Wheatley, M. A. Delivery of encapsulated Doxorubicin by ultrasound-mediated size reduction of drug-loaded polymer contrast agents. *IEEE Trans Biomed Eng* **2010,** *57*, (1), 24-8.
147. Fan, C. H.; Ting, C. Y.; Lin, C. Y.; Chan, H. L.; Chang, Y. C.; Chen, Y. Y.; Liu, H. L.; Yeh, C. K. Noninvasive, Targeted, and Non-Viral Ultrasound-Mediated GDNF-Plasmid Delivery for Treatment of Parkinson's Disease. *Sci Rep* **2016,** *6*, 19579.

148. Borden, M. A.; Caskey, C. F.; Little, E.; Gillies, R. J.; Ferrara, K. W. DNA and Polylysine Adsorption and Multilayer Construction onto Cationic Lipid-Coated Microbubbles. *Langmuir* **2007,** *23*, (18), 9401-9408.
149. Geers, B.; Lentacker, I.; Alonso, A.; Sanders, N. N.; Demeester, J.; Meairs, S.; De Smedt, S. C. Elucidating the mechanisms behind sonoporation with adeno-associated virus-loaded microbubbles. *Mol Pharm* **2011,** *8*, (6), 2244-51.
150. Sasaki, N.; Kudo, N.; Nakamura, K.; Lim, S. Y.; Murakami, M.; Kumara, W. R.; Tamura, Y.; Ohta, H.; Yamasaki, M.; Takiguchi, M. Ultrasound image-guided therapy enhances antitumor effect of cisplatin. *J Med Ultrason (2001)* **2014,** *41*, (1), 11-21.
151. ter Haar, G.; Shaw, A.; Pye, S.; Ward, B.; Bottomley, F.; Nolan, R.; Coady, A. M. Guidance on reporting ultrasound exposure conditions for bio-effects studies. *Ultrasound Med Biol* **2011,** *37*, (2), 177-83.
152. Escoffre, J. M.; Novell, A.; Piron, J.; Zeghimi, A.; Doinikov, A.; Bouakaz, A. Microbubble attenuation and destruction: are they involved in sonoporation efficiency? *IEEE Trans Ultrason Ferroelectr Freq Control* **2013,** *60*, (1), 46-52.
153. Fan, Z.; Chen, D.; Deng, C. X. Improving ultrasound gene transfection efficiency by controlling ultrasound excitation of microbubbles. *J Control Release* **2013,** *170*, (3), 401-13.

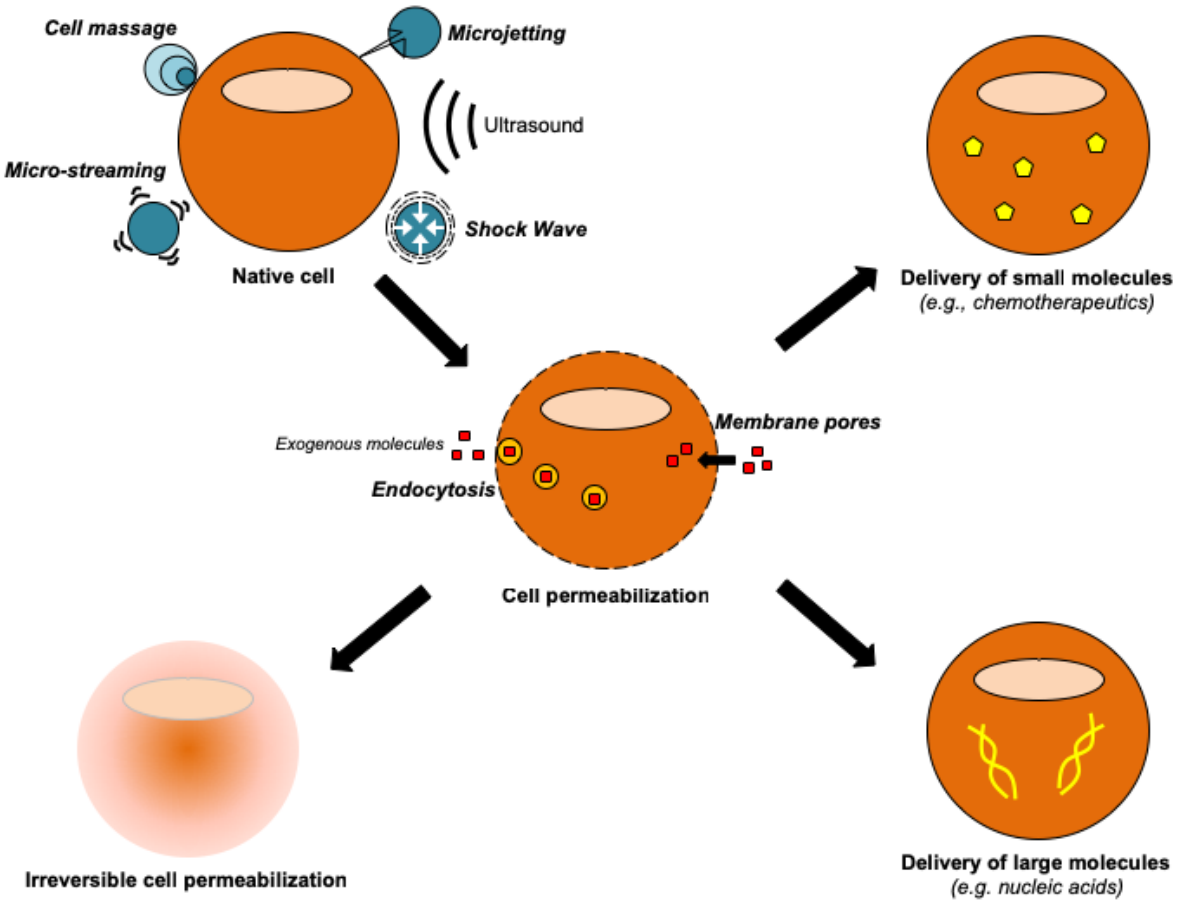

Biophysical mechanisms of cell membrane sonopermeabilization